3.3.4 Magnetic Flux Leakage Assessment of Specimen 2 Beams (S2-1, S2-2 and S2-3).

The following testing protocol was used to assess the pre-defined cross-sectional area losses of Specimen 2 beams using the Magnetic Flux Leakage Mobile Scanner.

(i) Locations of reinforcement and strands along the length of Specimen 2 beams were mapped out to define the scanning routes along the three beams.

(ii) Each reinforcement or strand was scanned 10 times. The objective of the test was to assess how the different pre-defined cross-sectional area losses along the reinforcement and strands could be detected by the Mobile scanner for quantification.

(iii) The assessed pre-defined percentage cross-sectional area losses were 5%, 10%, 15%, 20% and 30%.

(iv) The pre-defined length of wire cuts were 1 wire cut, 2 wires cut, 3 wires cut and 4 wires cut. The length of wire cuts were 0.25”, 0.5”, 0.75” and 1”.

Analysis of detailed results have been presented in section 4.3.2 which stipulates a study on magnetic flux leakage analysis on S2-1, S2-2 and S2-3

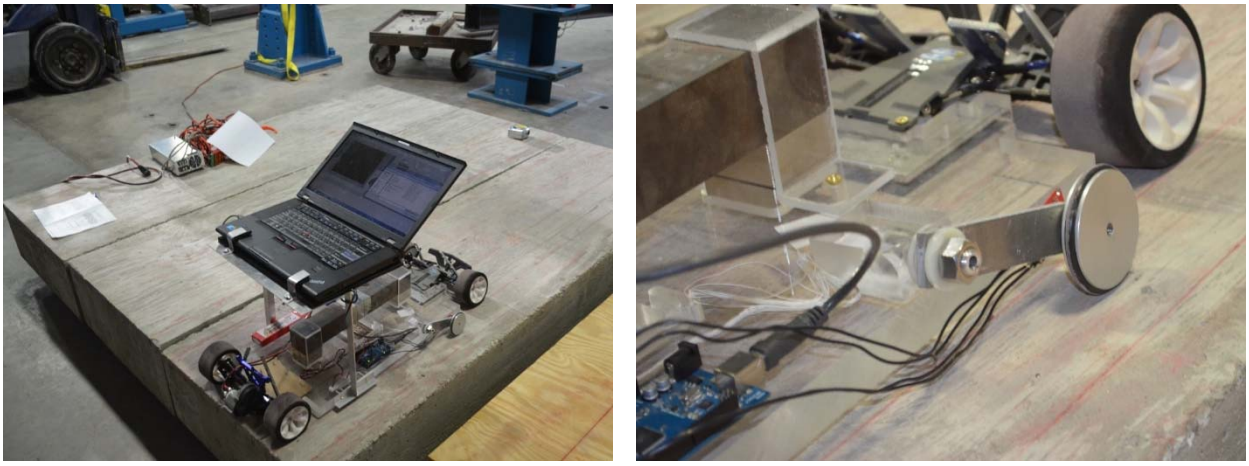

(a) MFL Mobile Scanner Setup *(b) Encoder for Distance Measurement*

Figure 3.60: MFL Mobile Scanner Assessing Cross-sectional Area loss/ Number and Length of Wire cuts for Specimen 2 Beams

3.4 Construction of Specimen 3 Beams for Simulation of Grouting Defects.

3.4.1 Construction Details (S3-1, S3-2, S3-3 and S3-4)

3.4.1.1 Design and Construction of Formwork and Building the Cages

Formwork was designed and constructed in the laboratory by research assistants and laboratory technical staff as shown in Figure 3.61. All reinforcements were cut, bent and installed in the laboratory as shown in Figure 3.66. Layout of simulated post-tensioned beams of S3-1, S3-2, S3-3 and S3-4 have been shown in Figures 3.62 – 3.65 depicting the various types of simulated conditions to be assessed using ultrasonic assessment. High density polyethylene (HDPE) corrugated duct of internal diameter 2.3 inches was used for the simulation of defects for S3-1 and S3-2. However S3-3 and S3-4 were simulated using corrugated steel duct of the same internal diameter. Figures 3.67-3.68 show final set-up of beams before placement of concrete.

(a) Cutting Plywood for Side Panels

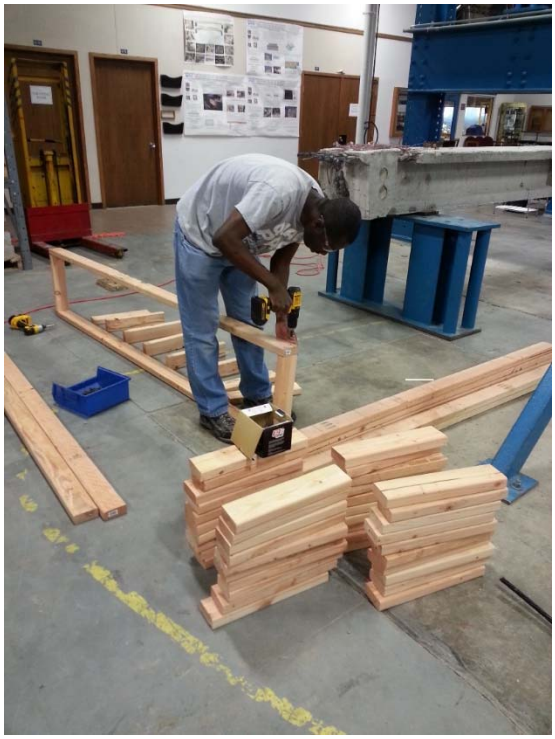

(b) Preparing Side Panels

Figure 3.61: Formwork Construction

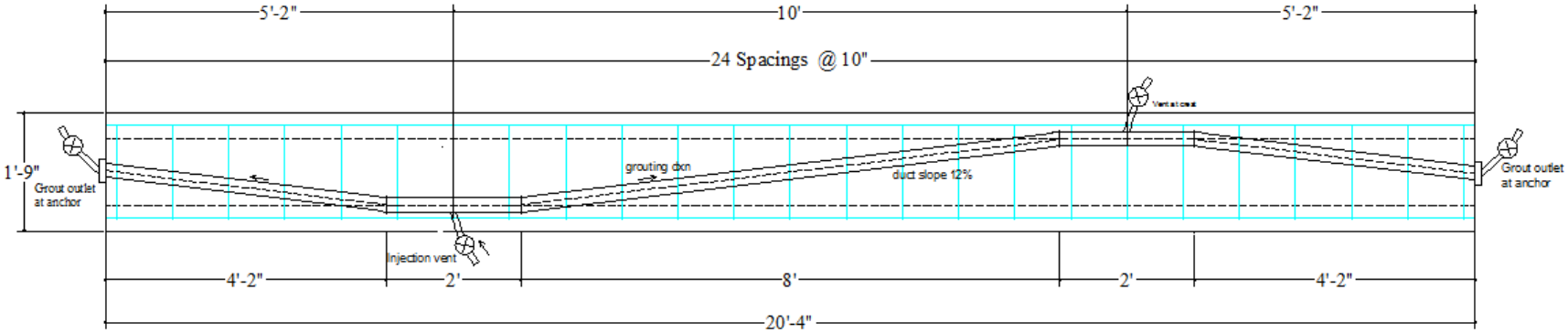

Figure 3.62: Configuration of S3-1 showing draped post-tensioned duct with simulated tendon paths in positive and negative moment regions and grout pumped in to check complete grout coverage at angle breaks

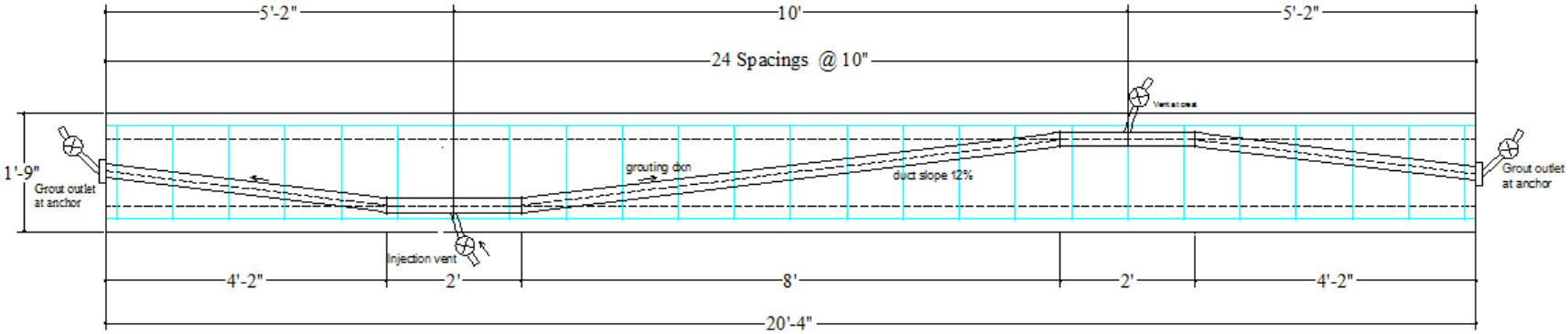

Figure 3.63: Configuration of S3-2 showing draped post-tensioned duct to be partially filled with water to be checked if the grout completely displaces the water.

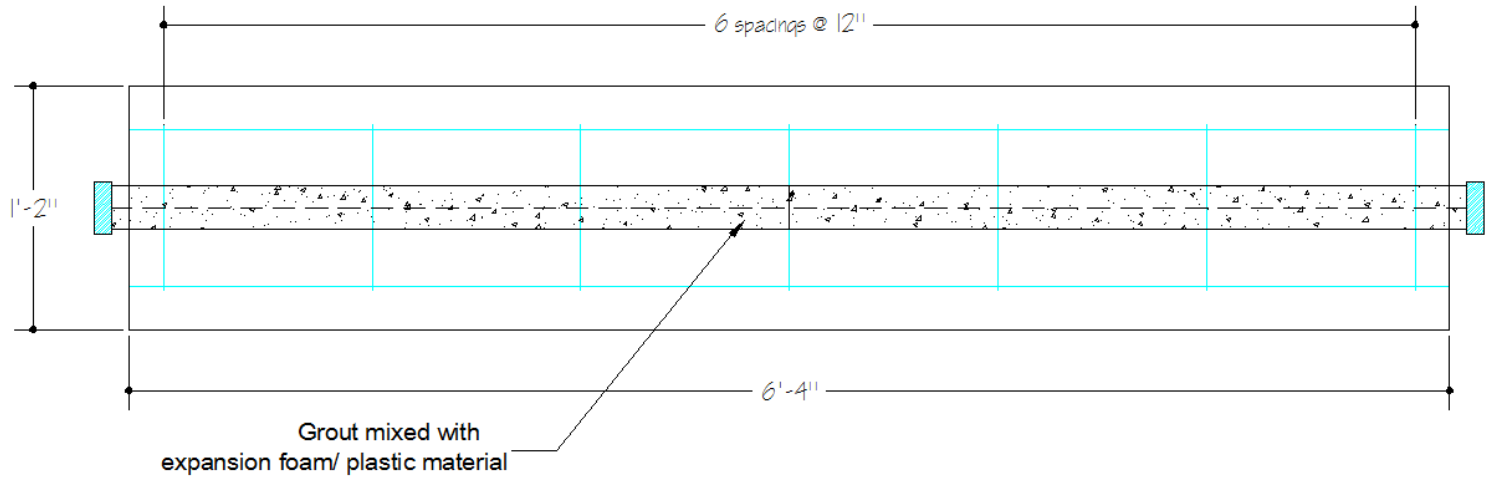

Figure 3.64: Configuration of S3-3 showing straight steel duct with grout mixed with expansion foam and plastic material

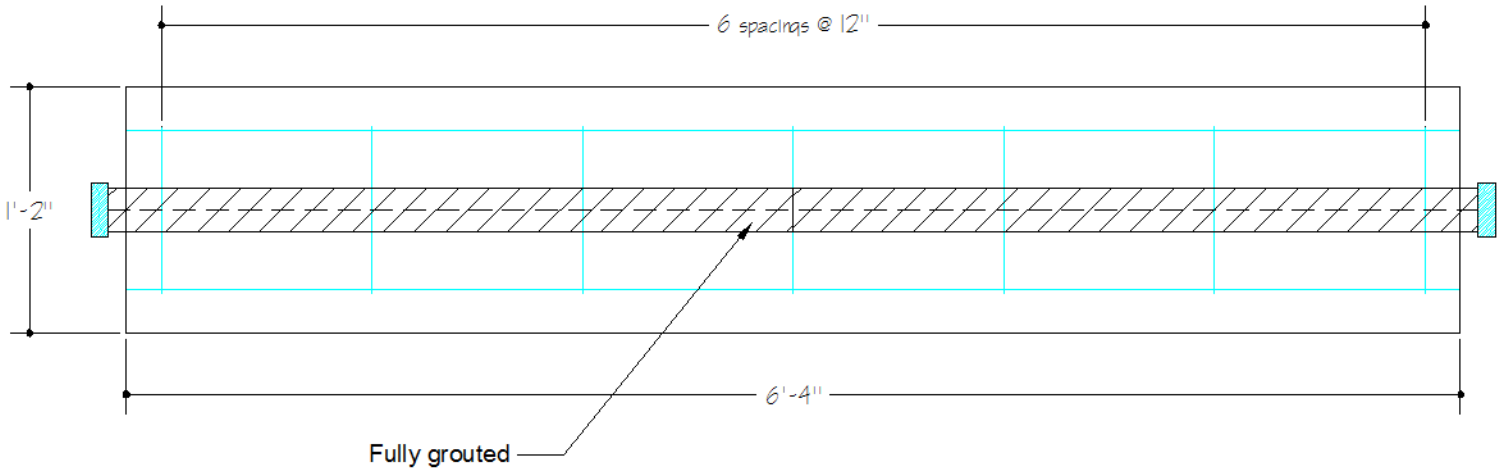

Figure 3.65: Configuration of S3-4 showing straight steel duct fully grouted in vertical position to be used as a reference to assess S3-1, S3-2 and S3-3

(a) : Bending of stirrups

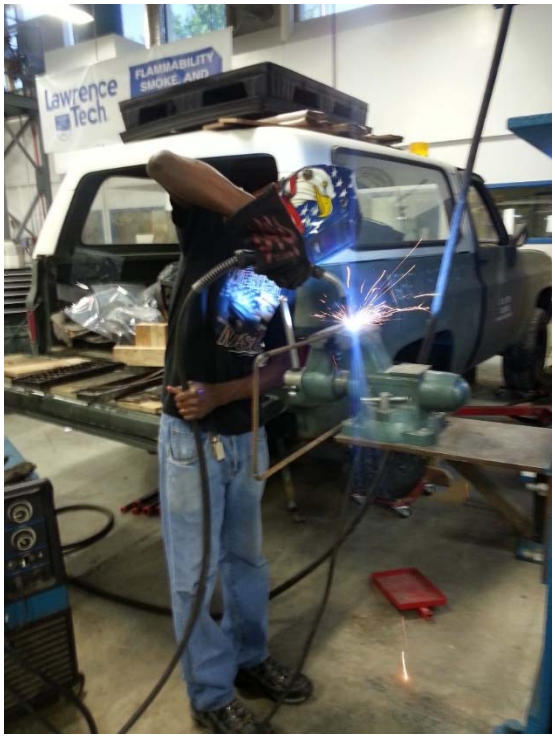

(b): Welding stirrups

(c): Draped Post-Tensioned Duct

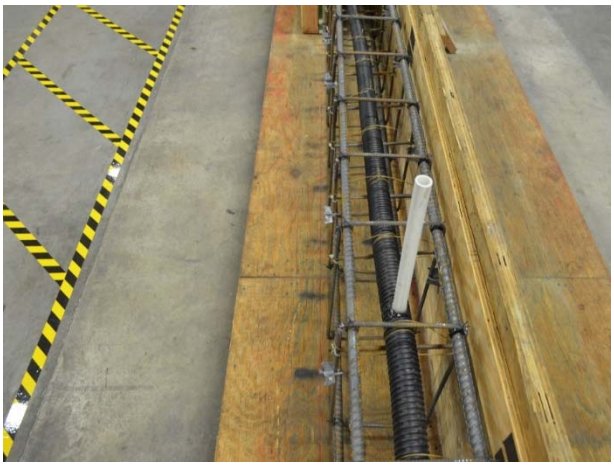

(d): Grouting Vent Connection at Crest

Figure 3.66: Rebar preparation and installation of draped post-tensioned duct

Figure 3.67: Setting Formwork

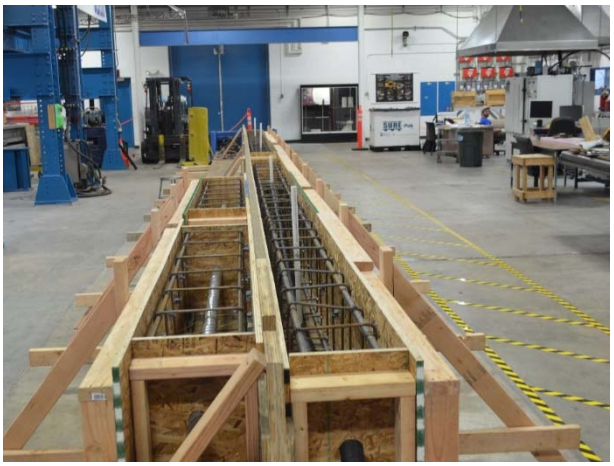

Figure 3.68: Beams Setup ready for casting

3.4.1.2 Concrete Placement

Concrete was placed into formwork in the laboratory by research assistants and laboratory technical staff as shown in Figure 3.69. A concrete slump of about 5-1/2 inches was recorded from the batch of concrete supplied by MCCOIG Materials, Detroit as shown in Figure 3.70. Formwork removal as part of the construction activities was carried out after 7 days. Formwork removal as well as extended curing after the 7th day have been shown in Figures 3.71 and 3.72.

Figure 3.69: Placing Concrete into Formwork.

Figure 3.70: Checking Concrete Slump

Figure 3.71: Removal of Formwork.

Figure 3.72: Curing of Beams

3.4.1.3 Grouting of Specimen 3 (S3-1, S3-2, S3-3 and S3-4)

Grouting of Specimen 3 beams was done using Cable Grout which is non-shrink sand free cement based grout that contains a unique two stage shrinkage compensation mechanism. Cable grout is non-metallic and contains no chloride. It contains silica fume to reduce permeability of the grout after setting. It has an initial set time of 3 hours and final set time of 8 hours which conforms to ASTM 191. It has a compressive strength of 3350 psi, 7510 psi and 8640 psi for 1 day, 7 days and 28 days respectively which conforms to ASTM C 942. It's bleed test as well as its permeability conforms to ASTM C 942 and ASTM C 1202 respectively. It was selected as the grouting material based on the above properties coupled with its flow ability. Kenrich GP-2HD Grout hand pump was used for the grouting of the simulated post-tensioned beams as shown in Figure 3.73. The GP-2HD has the following specifications.

Model	Kenrich GP-2HD
Pump Type	Single Diaphragm, Self-Priming
Power Source	Hand Operated
Output Capacity	6 gallons/minute (48cu.ft/hr)
Output pressure	0 to 15 psi
Hopper Capacity	0.62 cubic foot (4.6 gallons)
Discharge Head	10 foot Vertical Lift
Dimensions	23-1/2" x 12" x 23" high
Net Weight	21 pounds

Figure 3.73: Grouting Equipment set-up

3.4.1.4 Compressive Strength Testing of Concrete Cylinders

The average 28 day compressive strength of Specimen 3 beams was 8,540 psi. Strengths of various cylinders tested as well as the age in days of each of the cylinders when tested is shown in Table 3.2. The compressive strength was determined according to ASTM C39-05, Standard Test Method for Compressive Strength of Cylindrical Concrete Specimens.

Table 3.2: Compressive Strength Development using 6 inch by 12 inch Cylinders

Identification Number	Age of Specimen (days)	Compressive Strength (psi)
C1	7	5859
C2	7	5939
C3	7	5545
C4	14	6277
C5	14	6364
C6	14	6581
C7	21	6664
C8	21	6916
C9	21	7053
C10	28	8370
C11	28	8485
C12	28	8775

(a) 28-day Compressive Strength Test

(b) Failed Cylinder

Figure 3.74: Concrete Compressive Strength Testing

3.4.1.5 Ultrasonic Assessment of S3-1, S3-2, S3-3 and S3-4.

The following case studies were simulated for ultrasonic assessment.

- Polyethylene corrugated draped duct was used to simulate tendon paths in positive and negative moment regions and grout was pumped in to check complete grout coverage at angle breaks for S3-1.
- Polyethylene corrugated draped duct was filled partially with water to check if the grout completely displaced the water in the case of S3-2.
- Grout mixed with polystyrene (defects) was pumped into straight steel duct to assess how the ultrasonic scans could detect these defects for S3-3.
- S3-4 with steel duct was grouted vertically to ensure the duct was fully grouted to be used as a control for assessing grouting conditions of S3-1, S3-2 and S3-3.

Ultrasonic testing of Specimen 3 beams was perfomed using the following testing protocol.

(i) Scans of top and selected sides of each of the four beams with varied frequencies of 30, 40, 50, 60, 70, 80, 90 and 100 kHz were conducted before and after grouting to examine reflections from the post-tensioned ducts.

(ii) Localized scans were conducted at positive and negative moment regions for S3-1 and S3-2 with varied frequencies of 30, 40, 50, 60, 70, 80, 90 and 100 kHz before and after grouting

(iii) All scans were conducted with the longitudinal orientation of the ultrasonic equipment seated perpendicular to the longitudinal orientation of the post-tensioned ducts.

Figures 3.75 through 3.79 show scanning along various orientations along S3-1, S3-2, S3-3 and S3-4. Figures 3.80 and 3.81 show typical scans taken at designated locations along S3-1 and S3-3, respectively, before and after grouting to depict the differences in reflected intensities at the duct locations. It is clearly evident that reflected scan intensities at the duct locations had higher reflected intensities in the case of scans taken before grouting compared to those taken after grouting. Detailed analysis of scanned results have been discussed and shown in section 4.2.3 of this report.

Figure 3.75: Scanning Top of S3-1

Figure 3.76: Scanning Side of S3-1

Figure 3.77: Scanning Top of S3-2

Figure 3.78: Scanning Top of S3-3

Figure 3.79: Scanning Top of S3-4

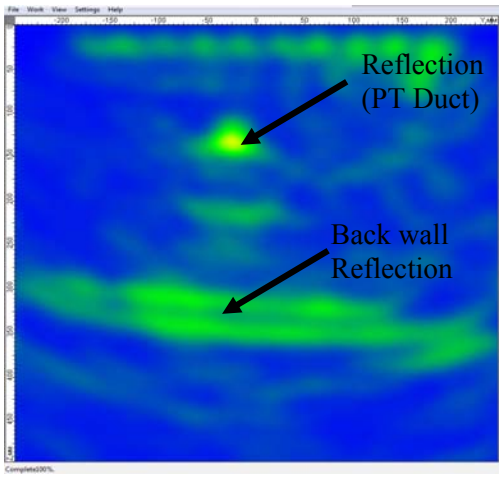

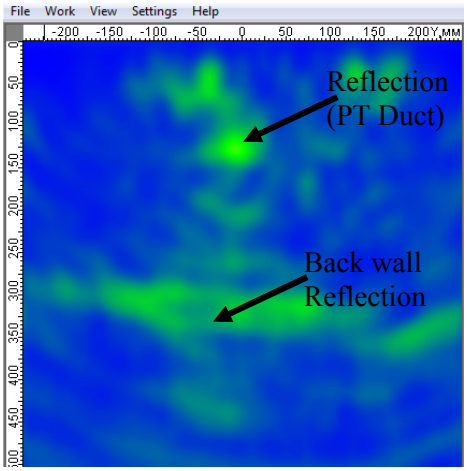

(a) Before Grouting *(b) After Grouting*

Figure 3.80: Examples of Scan Reflections from Side of S3-1 at 50kHz Before and After Grouting.

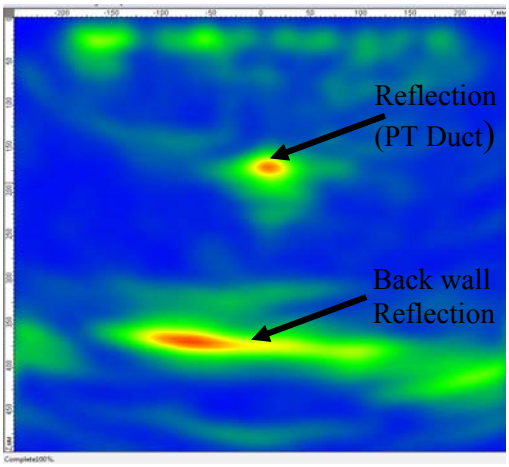

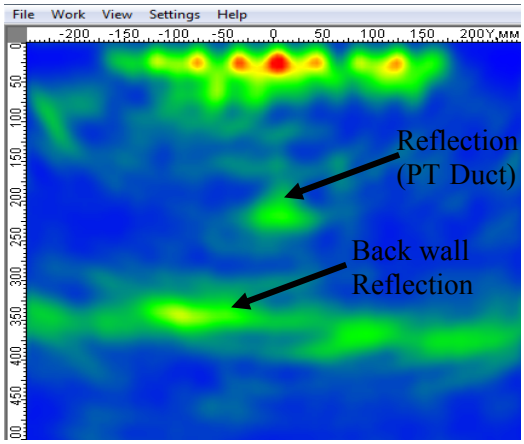

(a) Before Grouting *(b) After Grouting*

Figure 3.81: Examples of Scan Reflections from Side of S3-3 at 50kHz Before and After Grouting.

3.5 Evaluation of Salvaged Box Beams (J11, H6 and A1)

Salvaged box beams decommissioned by Kent County Road Commission, Grand Rapids in Michigan were inspected on May 6, 2013 to select beams for both residual flexural testing and nondestructive evaluation. The bridge was the Childsdale Avenue Bridge over Rouge River, 0.6 mile North of Kroes Street, Plainfield Twp. The following variables were considered in the selection of the salvaged beams for testing: corroded strands, spallings, patch ups, delamination and other defects. The three (3) beams selected reflected beams with good, average to worse condition; this was to verify the capability of selected NDE methods to evaluate varying levels of deterioration.

(a) Loading salvaged beam at Kent County

(b) Off-loading Salvaged Beams at CIMR, LTU

Figure 3.82: Salvaged Box Beams from Kent County

3.5.1 Experimental Program for Residual Flexural Testing

The bridge was decommissioned after 39 years of service due to deterioration. The study assessed how the observed deterioration in both concrete and prestressed strands had affected the overall flexural capacity of these beams. Each beam was 43 ft – 8 in long, 36 in wide and 21 in deep. The three box beams were randomly selected from different parts of the bridge and were likely to be subjected to varied levels of environmental exposure during their service life. The selected beams were made up of one interior and two exterior beams. Details of experimental procedure set-up for the box beams are as follows.

Prior to flexural testing, the following nondestructive methods were deployed: ultrasonic assessment for delamination and void detection; electro-chemical half-cell assessment for detecting corrosive environment; impact hammer assessment of surfaces to detect variations and potential delamination and magnetic flux leakage to determine loss of cross sectional area of reinforcement and strands.

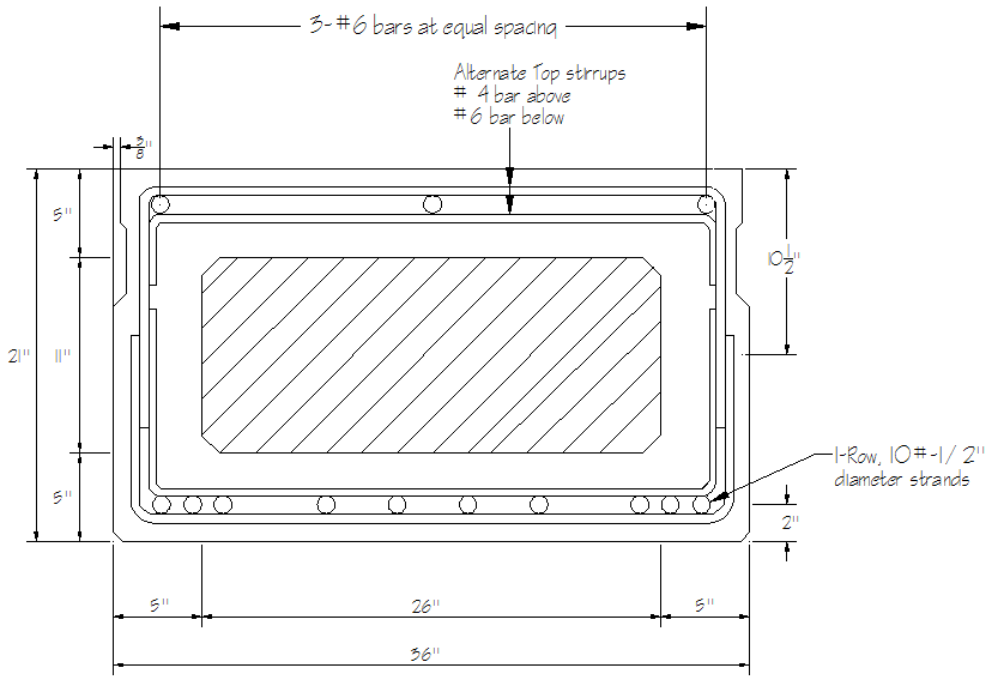

Figure 3.83: Typical Cross-section of Salvaged Beams

(Generated from construction drawings provided by Kent County Road Commission for Plainfield Bridge No. 6, Drawing No. 1074-3)

3.5.1.1 Design and Fabrication of a load spreader

A load spreader was designed and fabricated in the laboratory by research assistants and laboratory technical staff as illustrated in Figures 3.84 and 3.85

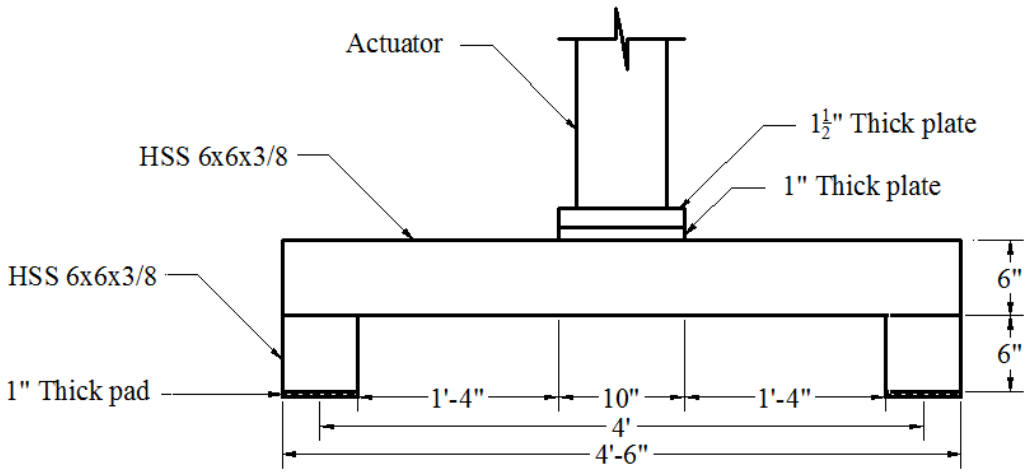

Figure 3.84: Fabricating Spreader

Figure 3.85: Fabricating Spreader

3.5.1.2 Instrumentation

The set-up of the flexural tests were designed to create a constant moment region at mid-span of the beams. The beams were tested using a 42 ft-4in span with two point loads applied two feet on either side of mid-span. The beams were supported on both ends on pads and the loads were applied to the beam through 36 in long and 6 in wide HSS cross-section across the width of the beam as shown in Figure 3.84.

The 21 in deep and 36 in wide box beams had hollow cavities of approximately 11 in by 26 in with post-tensioning duct at mid-span of the beams. The beams were prestressed with one-row of ten half inch diameter strands with ultimate capacity 270 k in the bottom flange with two strands debonded at each end of the beam. Three # six (6) bars at equal spacing were also located at the top flange with # four (4)stirrups at 9 in spacing for the first 3 ft -9 in from each beam end followed by a single stirrup spaced at 1 ft -10.5 in with subsequent stirrups at 2 ft spacing near the mid-span of the box beams.

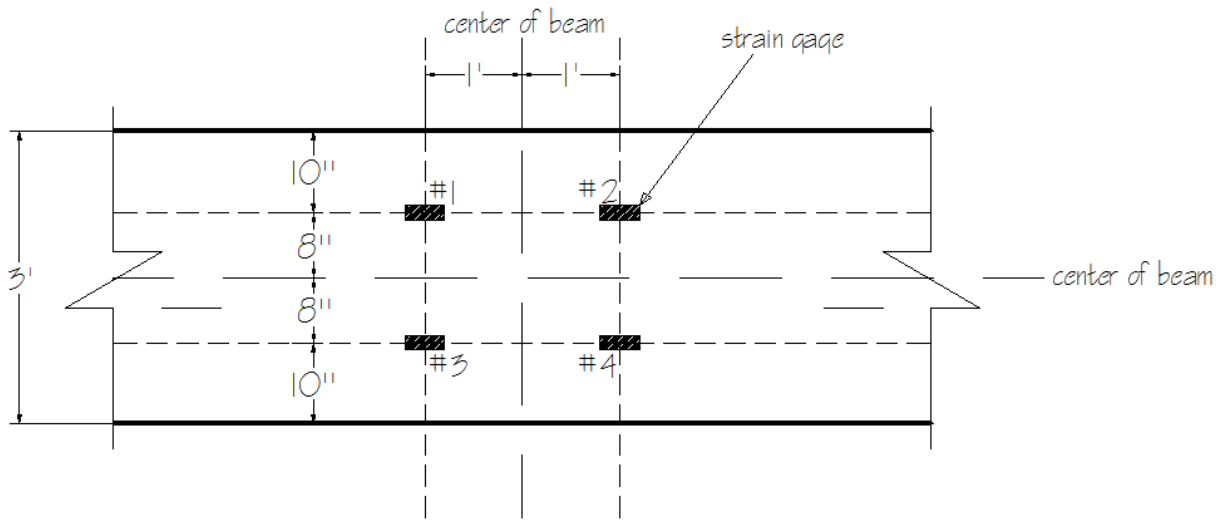

Figure 3.86: Layout of Strain Gages Installed on top Surface of Beams.

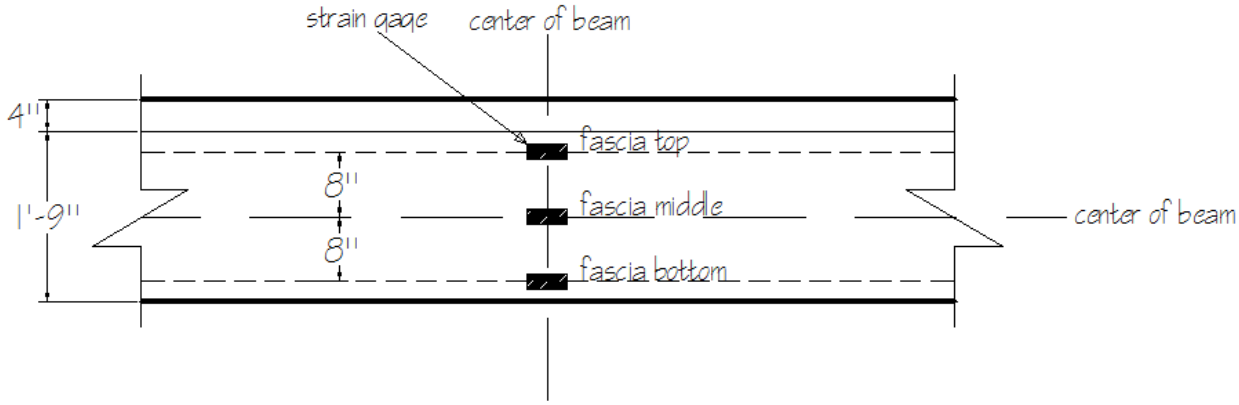

Figure 3.87: Layout of Strain Gages Installed on Fascia Side of Beams.

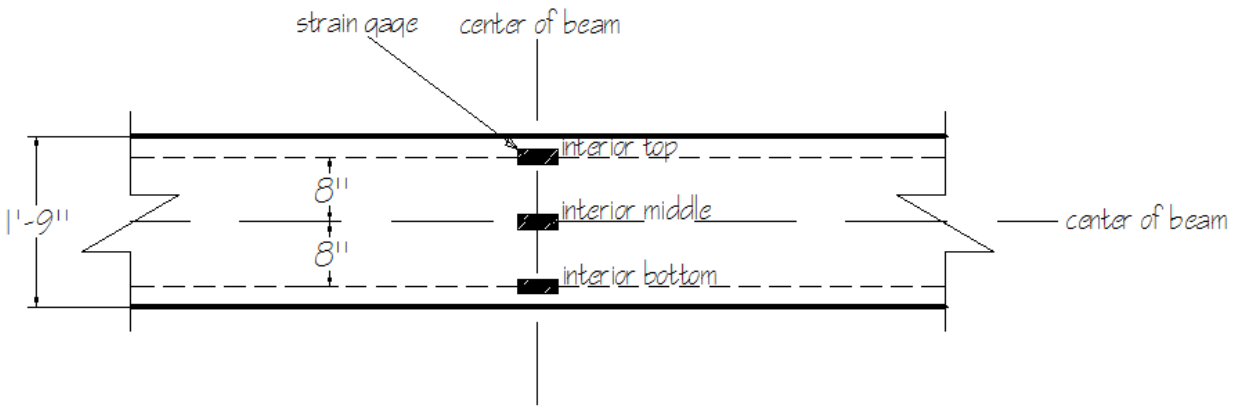

Figure 3.88: Layout of Strain Gages Installed on Interior Side of Beams.

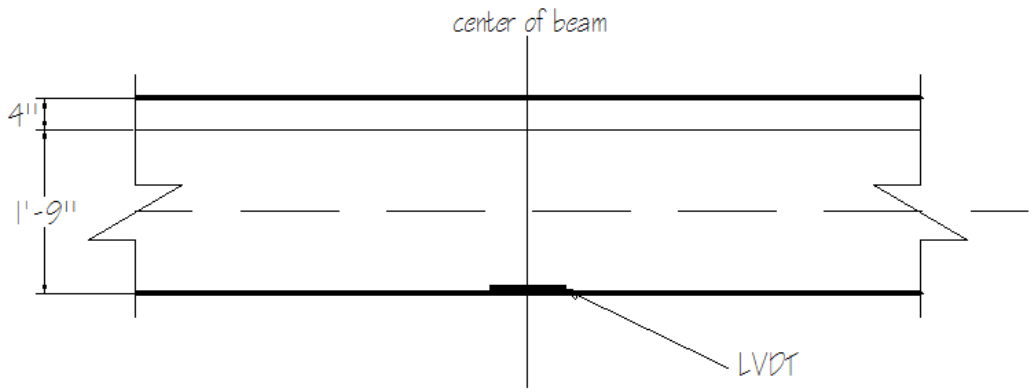

Figure 3.89: Location of LVDT Installed on Fascia Side of Beams

The instrumentation plan implemented on the beams included strain gages, linear string potentiometers and linear variable differential transducer (LVDT) as shown in Figures 3.86 through 3.89. Ten (10) resistance strain gages were applied at the mid-span of each box beam. Four (4) strain gages (N2A-06-20CBW-350) were applied to the top of the beams equally spaced in rows of two (2), 12 inches on each side from the center of the beams as illustrated in Figure 3.86. Three (N2A-06-20CBW-350) were placed at the fascia and interior sides and they were equally spaced at approximately 8 inches from top to bottom as shown in Figures 3.87 and 3.88. All strain gages measured longitudinal strain in the beams. Two string potentiometers were attached to the middle bottom portion of the beams, one under each point load to measure the vertical deflection. The precision of the employed string port was ±0.0025mm (0.0001 in). Additional two (2) LVDT's were also placed one on each bottom side at the mid-span as shown in Figure 3.89. Data was collected and saved continuously throughout the test. Four point loading was applied to the salvaged beams at cyclic loading increments of 4 kips up to failure. Initiated

cracks due to loading were mapped out after each load increment and the cracks were observed as the crack widths and lengths increased in each load cycle. Figures 3.90 and 3.91 show typical set-up of residual flexural set-ups for 4 and 8 kips. Set-up of salvaged box beams before and after failure are shown in Figures 3.92-94.

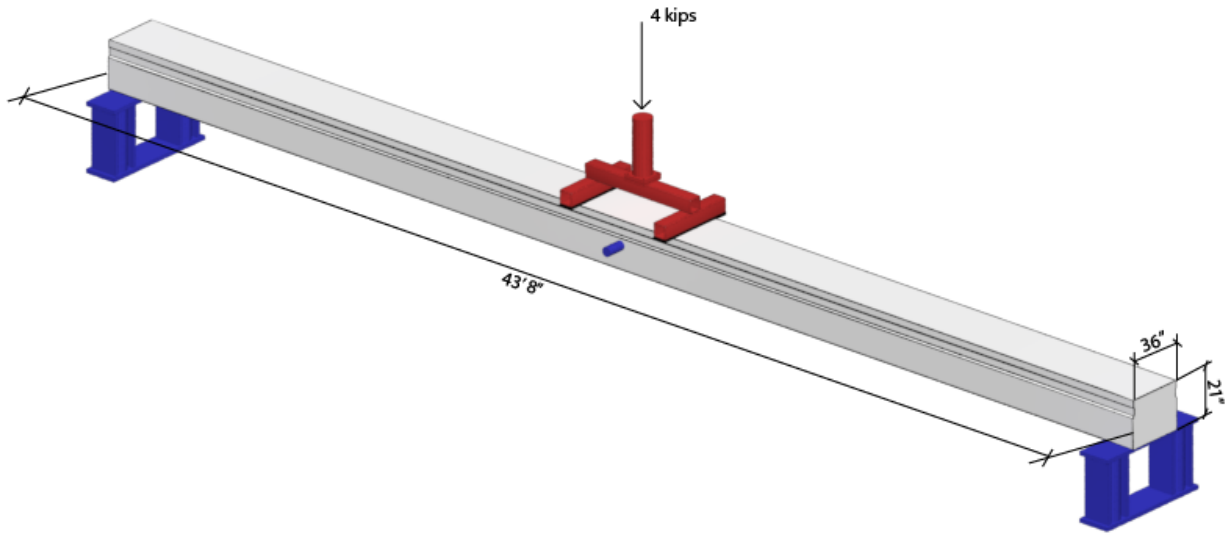

Figure 3.90: Box Beam Residual Flexural Set-up at 4 kips Loading.

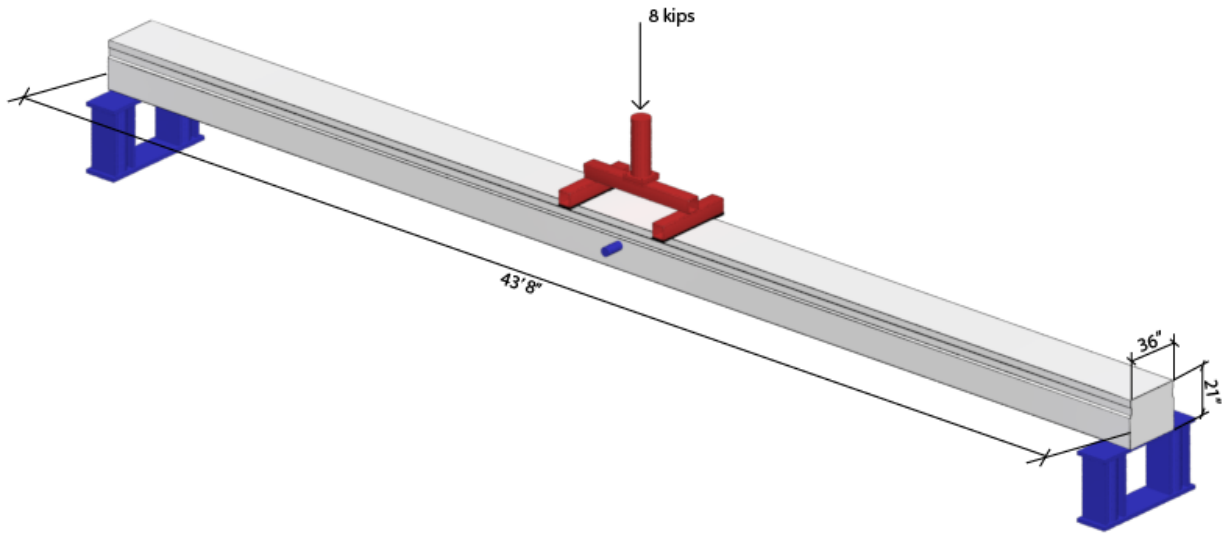

Figure 3.91: Box Beam Residual Flexural Set-up at 8 kips Loading.

(a) *Set-up for Salvaged Beam 1 (J11)* *(b) Salvaged Beam 1 (J11) after failure*.

Figure 3.92: Set-up for Salvaged Box Beam J11 before and after failure.

(a) Set-up for Salvaged Beam 2 (H6) *(b) Salvaged Beam 2 (H6) after failure*

Figure 3.93: Showing Set-up for Salvaged Box Beam H6 before and after failure.

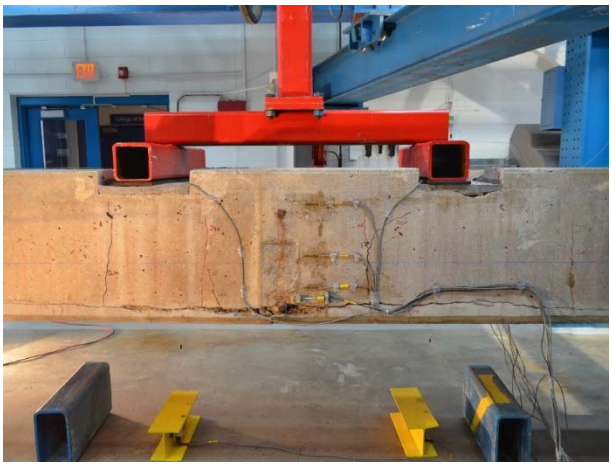

(a) Set-up for Salvaged Beam 3 (A1)

(b) Set-up for Salvaged Beam 3 (A1)

(c) Salvaged Beam 3 (A1) during Failure

(d) Salvaged Beam 3 (A1) after Failure

Figure 3.94: Showing Set-up for Salvaged Box Beam A1 before and after failure.

3.5.2 Electro-chemical Testing of Salvaged Beams Using Canin

Grids of 6 in x 6 in were drawn at the bottom of the salvaged beams for testing. The tests were conducted at the intersection of the grids as illustrated in Figure 3.95. The average results for salvaged box beam 1 (J11) varied from -130mV which according to ASTM 876 has 5% chance of corrosion to -460mV which has a chance of 95% of corrosion while the average results for salvaged beam 2 (H6) varied from +12mV which according to ASTM 876 has 5% chance of corrosion to -583mV which has visible evidence of corrosion. The average results for salvaged beam 3 (A1) varied from +10mV which according to ASTM 876 has 5% chance of corrosion to -393mV which has 95% chance of corrosion. The data collected from the canin have been used to map up the level

of corrosion of prestressing strands along the length of the beams. Potential maps as well as cumulative frequency curves have been presented in Section 5.1.2 of this report. Values of half-cell potential were used to analyze the chance of corrosion along the bottom of the salvaged beams using the ASTM C876 guidelines, as it is shown in Table 3.3.

Table 3.3: Interpretation of half-cell potential values as per ASTM C876

Potential difference (mV)	Chance of rebar being corroded
< -500	Visible evidence of corrosion
-350 to -500	95%
-200 to -350	50%
> -200	5%

Figure 3.95: Electro-chemical Half-cell of salvaged beam

3.5.3 In-situ Hardness Testing of Salvaged Beams Using Schmidt Hammer

Grids of 6”x12” were drawn along the bottom of the salvaged beams tested in CIMR laboratory dividing the surface into approximately 175 rectangles, and 10 measurements were taken in each of this rectangles as shown in Figure 3.96. The method used to estimate the Q value of each area was the mean of the 10 measurements.

The hammer computer program “ProVista” relates the rebound coefficient to the in-situ compressive strength. As the rebound value depends on the concrete in-situ hardness, the energy that the concrete absorbs can be correlated with its compressive strength. The relationship between energy absorbed and compressive strength was determined using a referencing curve, and in this project the curve used was the lower 10th percentile curve that comes with the instrument program. The following deductions were used a low rebound number indicates that the concrete is weak and has low compressive strength, on the other hand, a high Q value is an evidence a hard and strong surface with higher compressive strength. An average in-situ compressive strength of 6100 psi was estimated for the salvaged beams.

Figure 3.96: Schmidt Hammer Testing for Salvaged Beam 1(J11)

3.5.4 Ultrasonic Assessment of Salvaged Beams J11, H6 and A1

Ultrasonic assessments were conducted on the three salvaged box beams at the Center for Innovative Materials Research (CIMR). The following testing protocol was developed and used for evaluation of the salvaged beams.

(i) Complete scan of the two longitudinal sides and the bottom of the beams with varied frequencies of 30, 40, 50, 60, 70, 80, 90, and 100 kHz to examine how the side webs and bottom flange thicknesses were detected with the above frequencies

(ii) Localized scans on strand locations along the length of the beam with the help of MDOT drawings as shown in Figure 3.85 and profometer with frequencies of 30, 40, 50, 60, 70, 80, 90, and 100kHz

(iii) Localized scans on corroded strands, (strands were located by visual inspection depending on the results of electro-chemical analysis) with frequencies of 30, 40, 50, 60, 70, 80, 90 and 100kHz

(iv) Localized scans on un-corroded strands, (strands were located by visual inspection depending on the results of electro-chemical analysis) with frequencies of 30, 40, 50, 60, 70, 80, 90, and 100 kHz

Figure 3.97 show assessments along various locations of the salvaged box beams, and results and discussion of the assessments are presented in section 5.1.1 of this report.

(a) Bottom of salvaged box beam J11

(b) Side of salvaged box beam J11

(c) Bottom of salvaged box beam H6

Figure 3.97: Ultrasonic Assessment of Salvaged Box Beams

3.5.5 Magnetic Flux Leakage Assessment of J11, H6 AND A1

Magnetic flux leakage assessment was conducted along the 10 bottom strands of the salvaged box beams where the locations of the bottom strands were mapped out as detailed in Figure 3.101. The bottom of the box beams were divided into three sections for assessment. The middle section was assessed before failure of the box beams whiles the two end sections were assessed after failure. The scanning configuration of the bottom of the box beams have been detailed in Figures 3.98 – 3.100, indicating scanned and unscanned sections as well as sections scanned before failure of box beams. The unscanned sections represents areas of delaminated concrete surfaces. The data analysis will be inconclusive if the MFL reference surface is uneven.

A plywood support structure was installed along the length of both sides of the beams to allow the MFL mobile scanner to scan the outer strands, (S1 through S3 and S8 through S10). Figure 3.102 shows the MFL mobile scanner scanning strand S5 on the north half of box beam J11. Strands along bottom beams of H6 and A1 were assessed in a similar manner as detailed in Figures 3.99 and 3.100. Results and discussions of the assessment are presented and discussed in section 5.1.4 of this report.

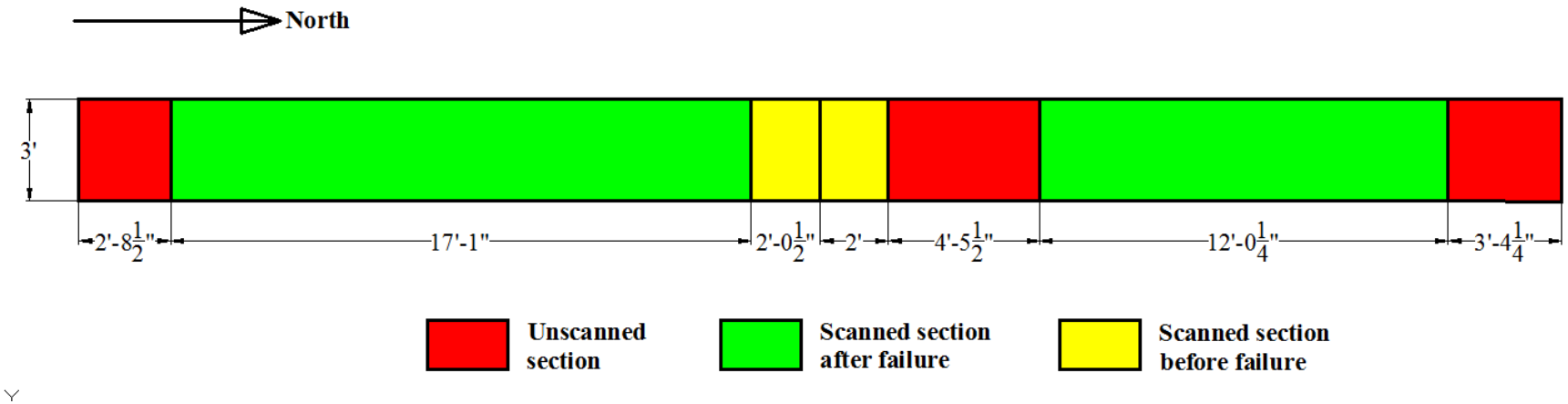

Figure 3.98: Scanning Configuration at the Bottom of Box Beam J11. (Generated from construction drawings provided by Kent County Road Commission for Plainfield Bridge No. 6, Drawing No. 1074-2)

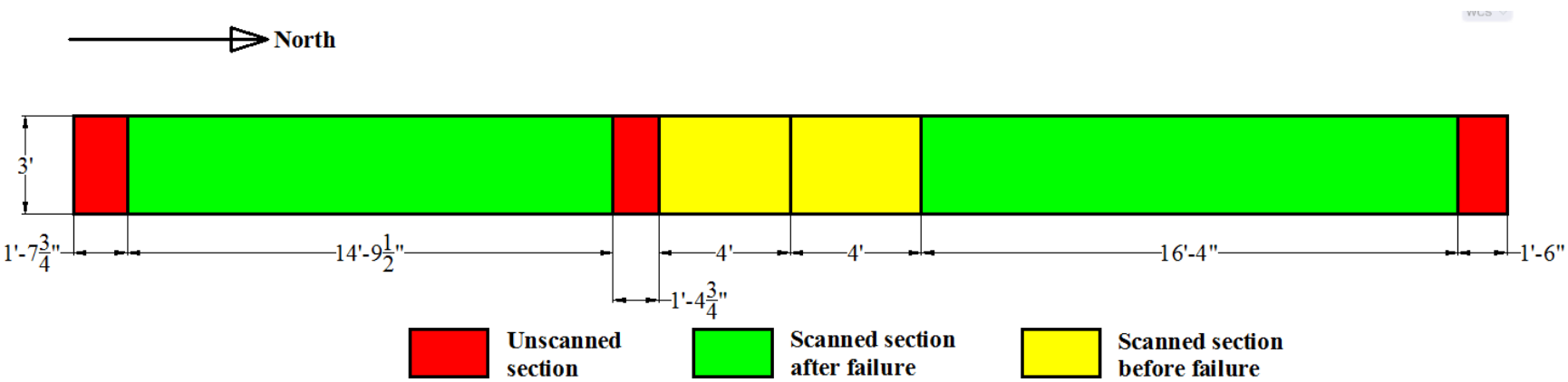

Figure 3.99: Scanning Configuration at the Bottom of Box Beam H6. (Generated from construction drawings provided by Kent County Road Commission for Plainfield Bridge No. 6, Drawing No. 1074-2)

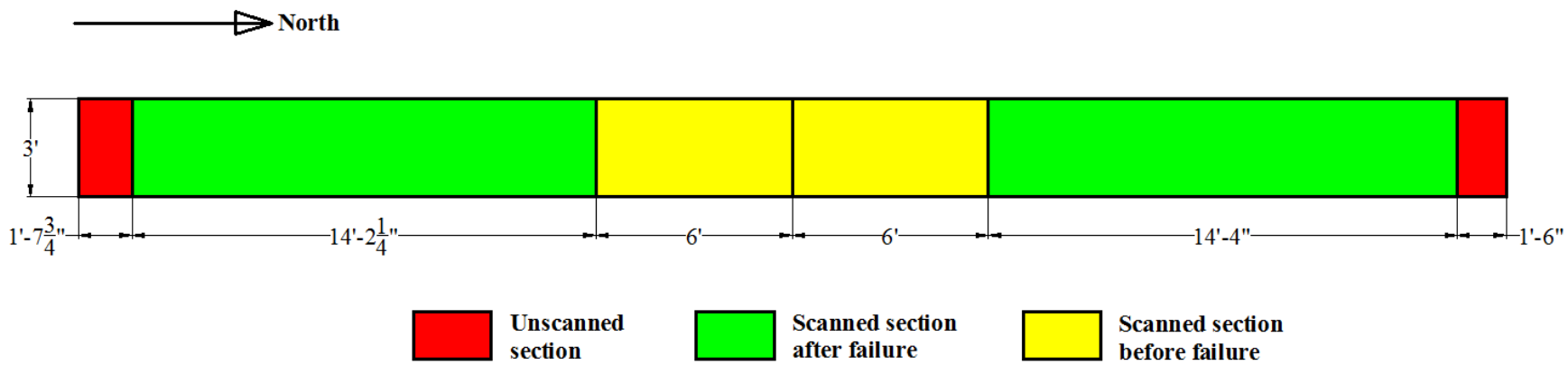

Figure 3.100: Scanning Configuration at the Bottom of Box Beam A1. (Generated from construction drawings provided by Kent County Road Commission for Plainfield Bridge No. 6, Drawing No. 1074-2)

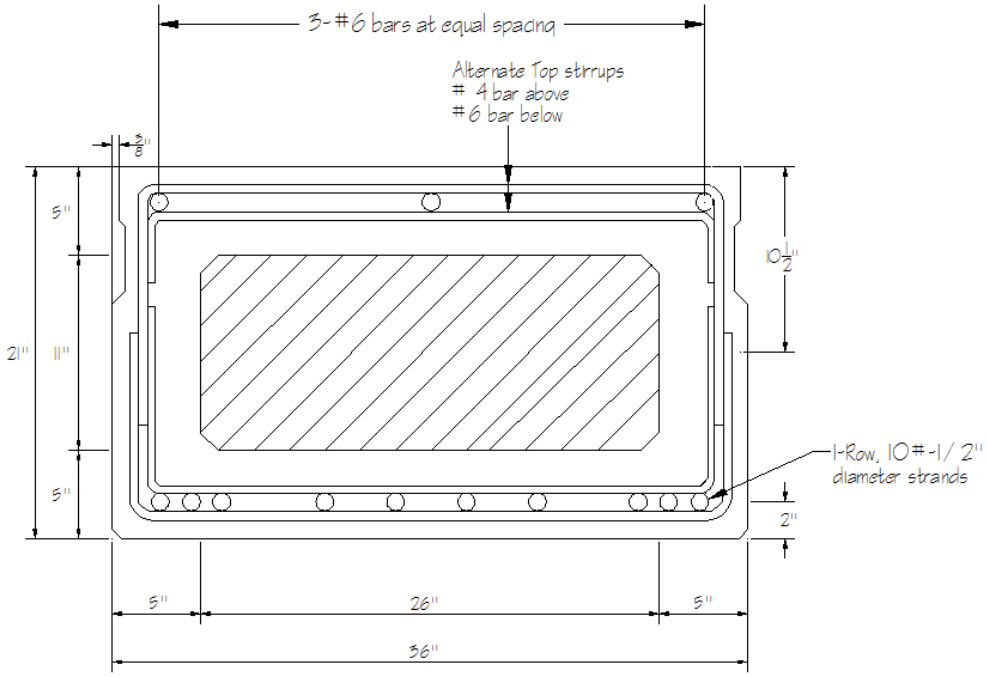

Figure 3.101: Typical Cross-section of Salvaged Beams

(Generated from construction drawings provided by Kent County Road Commission for Plainfield Bridge No. 6, Drawing No. 1074-3)

Figure 3.102: Scanning Strand #5 (S5) on North Half of Savage Beam with MFL Mobile scanner

3.6 NDT Field Testing

3.6.1 US-131 over Muskegon River, Southbound Lanes

Nondestructive assessment was conducted on segments of US-131 over Muskegon River, southbound lanes, 6 miles South of Big Rapids. Ultrasonic assessment was used for delamination and void detection; electro-chemical half-cell assessment was used for detecting corrosive environment, and magnetic flux leakage assessment was used to determine loss of cross sectional area of reinforcement and strands. The field inspections were carried out from July 22 to 24, 2014. The following reference plan sheets were used from US-131 MDOT Job Number 16246A: B01-1, B01-4, B01-5, B01-6 and B01-7.

The MDOT bridge construction project has the following identification details.

Michigan Project	FFD 131-3(318)
Control Section	FF 54014
Job Number	16246A

The bridge was located in Mecosta Township within Mecosta County. Details of the field assessments are presented below. A segment numbering system used for this assessment were all referenced to the north abutment of US-131 over Muskegon River.

- Ultrasonic assessment on transverse post-tensioned duct located in Segments 2 and 4.
- Ultrasonic assessment on longitudinal post-tensioned duct #24 between piers 1 and 2 and anchorage at ends of duct.
- Magnetic flux leakage (MFL) scanning on selected bottom flange within segment 2
- Ultrasonic assessment on selected bottom flange within segment 2 to support MFL
- Ultrasonic assessment on web within segment 2 along longitudinal and transverse rebar to check for pockets of void.
- Electrochemical half-cell assessment on selected web segment within segments 2 and 4.

3.6.1.1 Ultrasonic Assessment on Transverse Post-tensioned Ducts located in Segments 2 and 4

One duct each was selected and located within segments 2 and 4 using:

- US-131 plan sheets for Job Number 16246A: B01-1, B01-4 and B01-6
- Ground Penetrating Radar (GPR)

Figure 3.103: US-131 over Muskegon River (SB)

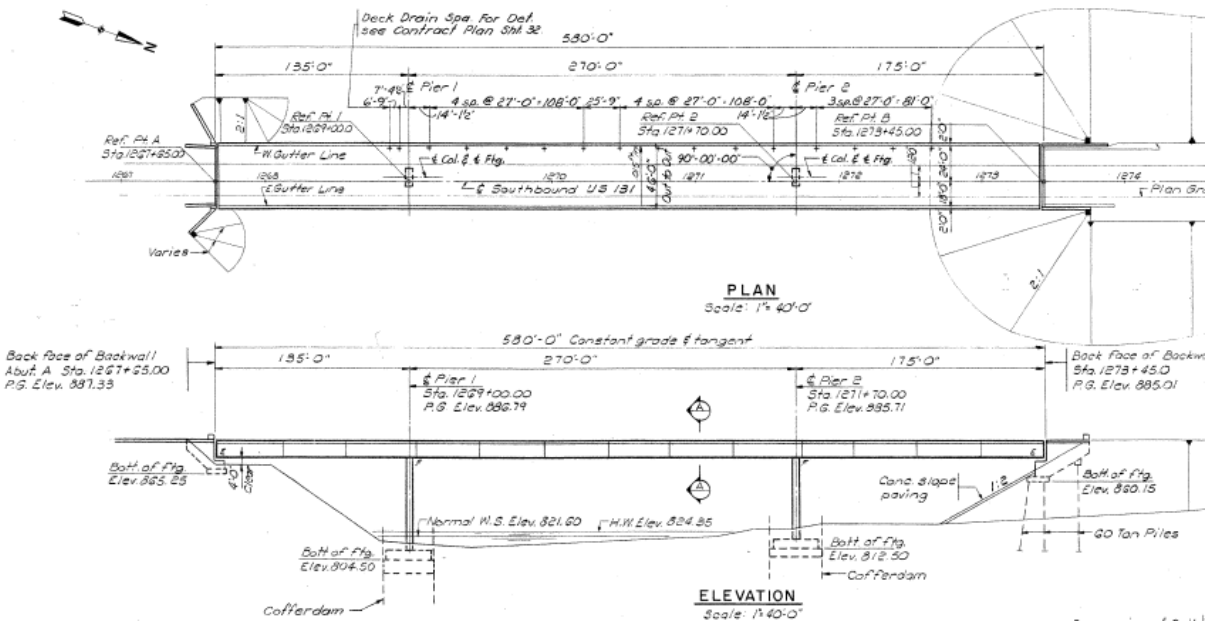

Figure 3.104: Plan and Elevation of US-131 over Muskegon River (SB)

Ultrasonic assessment on transverse post-tensioning ducts were conducted at a standard frequency of 50 kHz. Scans were done perpendicular to the direction of the transverse post-tensioning ducts

and were restricted to the interior portions of the segments. The length of scanning on each selected duct was approximately 21 ft – 6 in and each duct was scanned three (3) consecutive times to aid in analysis of the scanned results. Figure 3.105 show scanning along transverse duct in segment 2 and the location of the transverse duct have be highlighted in Figure 3.106 from drawing extracted from plan sheet B01-4. Figure 3.107 shows typical scan results along transverse post-tensioning duct showing location of duct and backwall reflection from the top flange. Detailed results and analysis are presented in section 5.3.1.1 of this report.

Figure 3.105: Scanning on Transverse Post-tensioning Duct within Segment 2

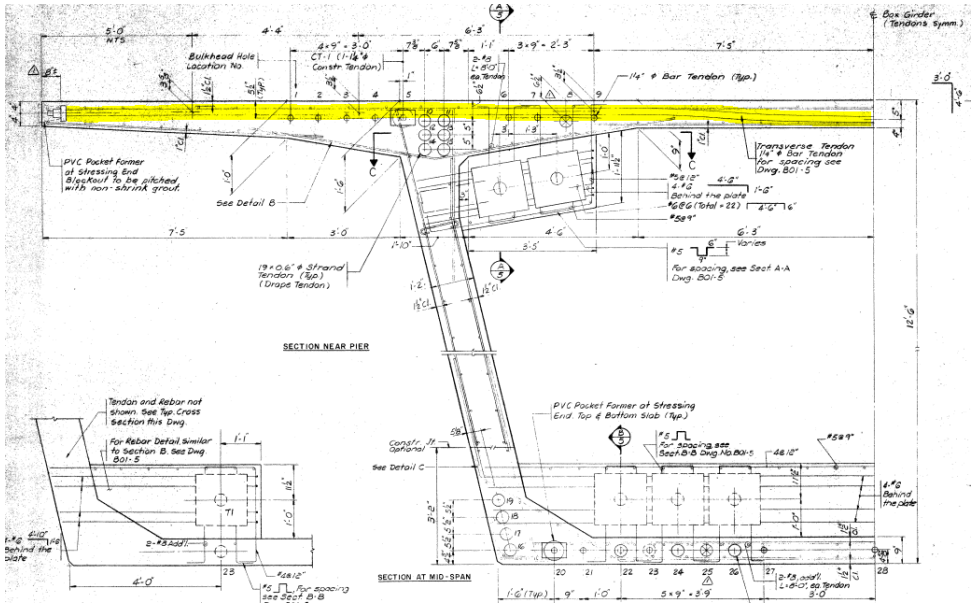

Figure 3.106: Highlighted Location of Transverse Post-tensioning Duct, Plan Sheet BO1-4

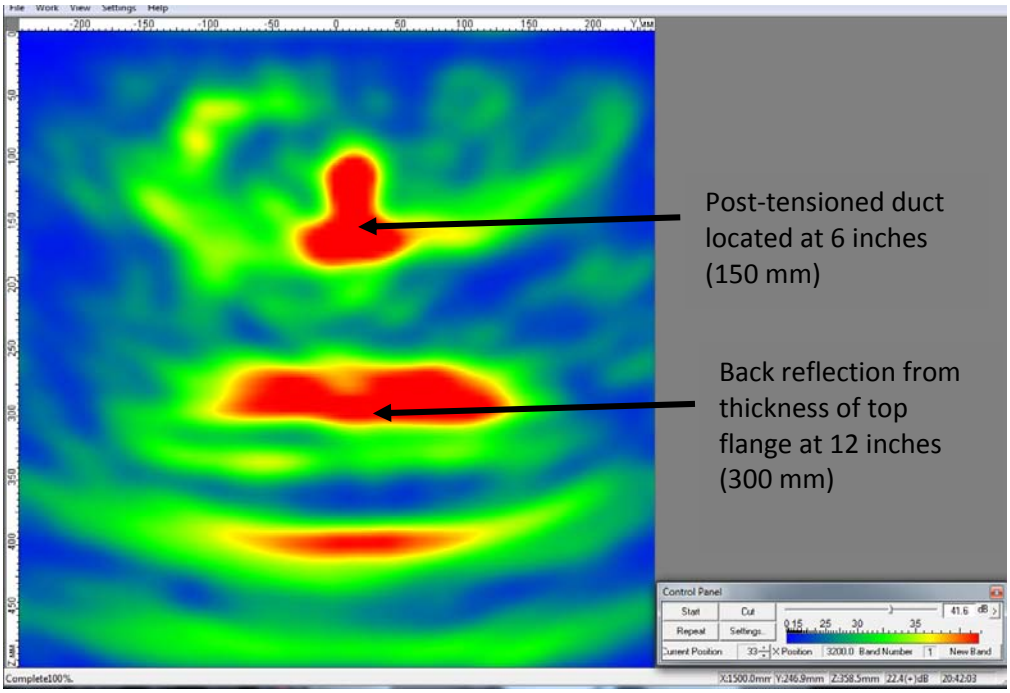

Figure 3.107: Typical Scan Result along Transverse Post-tensioning Duct, showing location of duct and back reflection from thickness of Top Flange.

3.6.1.2 Ultrasonic assessment on longitudinal post-tensioned duct Number 24 between piers 1 and 2 and anchorages at the ends of the duct.

Post-tensioned Duct Number 24, between piers 1 and 2 was selected and located using:

- US-131 plan sheets from Job Number 16246A: B01-4 and B01-5.
- Ground Penetrating Radar. (GPR)

Ultrasonic assessment on longitudinal post-tensioning duct #24 as well as the anchorages at the ends were conducted at a standard frequency of 50 kHz. Scans were done perpendicular to the direction of the longitudinal post-tensioning ducts and scans were restricted to the interior portions of the segments. The length of scanning spans between Pier 1 and 2 and the duct was scanned three (3) consecutive times for analysis of the scanned results. Scanning was done in the north–south direction, from pier 1 towards pier 2. Figure 3.108 shows scanning being conducted along longitudinal duct #24 and anchorages at the ends. Figures 3.109 and 3.110 show the southbound cros-section, showing post-tensioned duct number 24 extracted from plan sheet BO1-4 and tendon anchorage details for bottom slab extracted from plan sheet BO1-5. Typical scan

reflection showing location of duct and back-wall reflections from the thickness of the bottom flange are shown in Figure 3.111. Detailed results and analysis have been presented in section 5.3.1.2 of this report.

Figure 3.108: Scanning on Longitudinal Post-tensioned Duct #24 and Anchorages

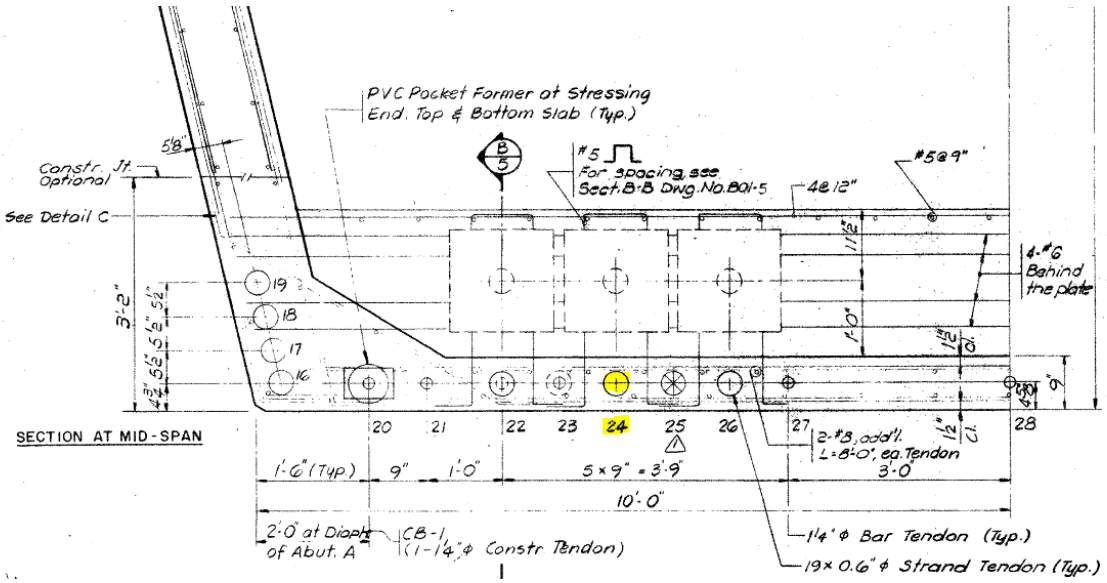

Figure 3.109: Cross-section of SB, highlighting Duct #24, Plan Sheet BO1-4

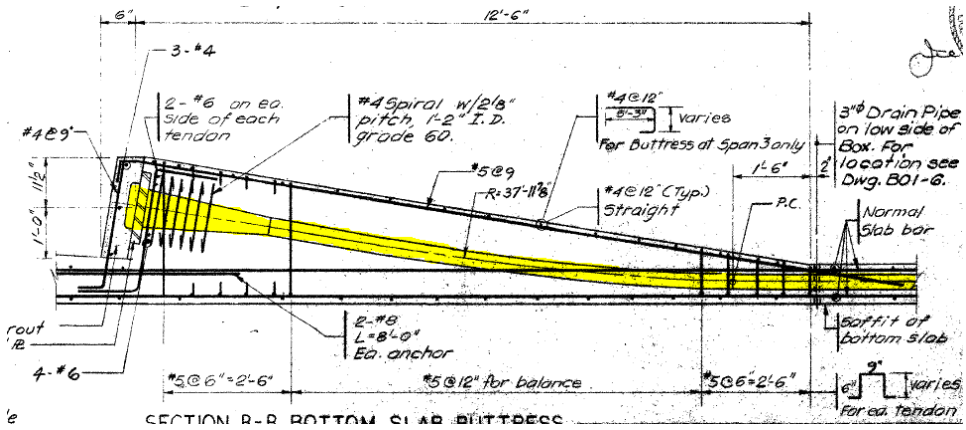

Figure 3.110: Tendon anchorage details for bottom slab, Plan Sheet BO1-5

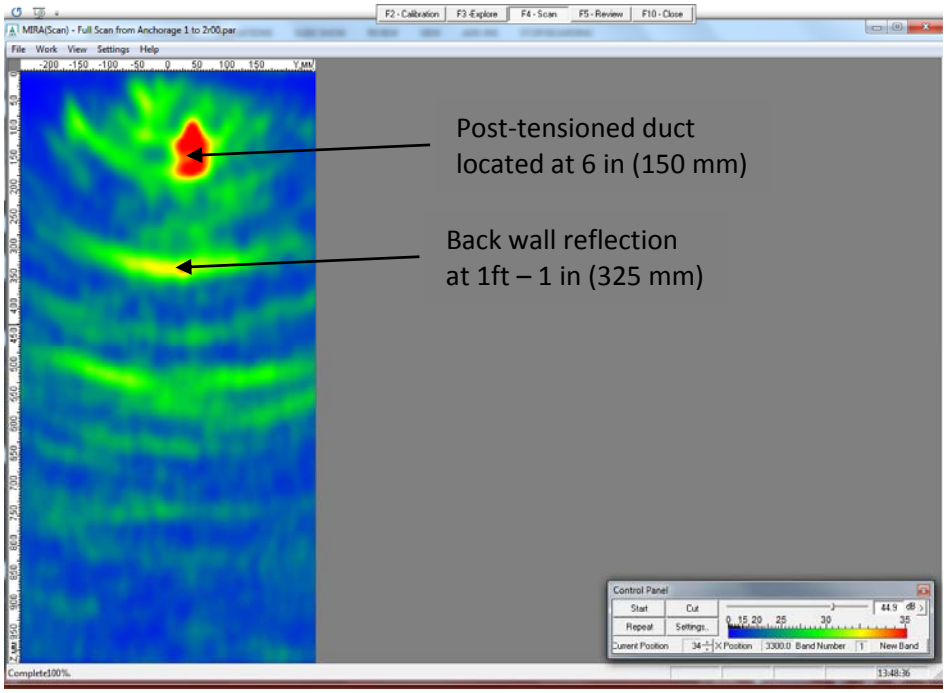

Figure 3.111: Typical Scan along Longitudinal Post-tensioning Duct 24, showing location of duct and back reflection from thickness of bottom flange.

3.6.1.3 Ultrasonic Assessment on Selected Bottom Flange within Segment 2

Ultrasonic assessment was conducted within Segment 2 to support Magnetic Flux Leakage (MFL) assessment. Grids were mapped out along the longitudinal and transverse top rebar of the bottom flange using US-131 plan sheets from Job Number 16246A: sheet B01-7 and Ground Penetrating Radar. Scanning was conducted along reinforcement locations, to detect the presence of delaminations and possible corrosion around reinforcement. Three scans were conducted along the selected reinforcement locations. Figure 3.112 shows a typical cross-section of segment showing bottom flange and web rebar details extracted from plan sheet BO1-7. Segments arrangement showing location of segment 2 between Abutment A and Pier 1 extracted from plan sheet BO1-1 are shown in Figure 3.113. Detail results and analysis are presented in Section 5.3.1.3 of this report.

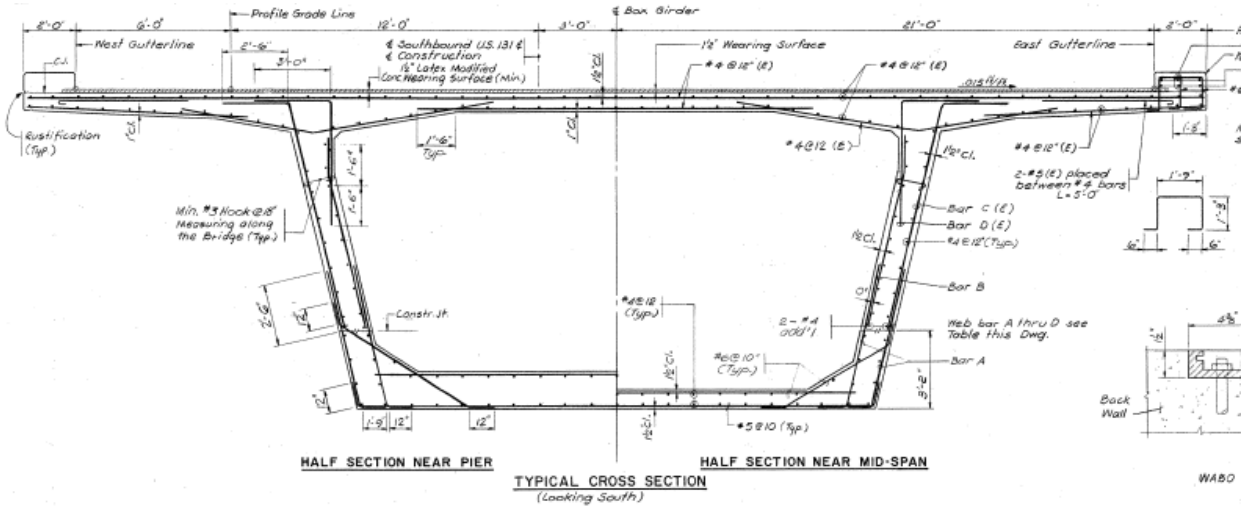

Figure 3.112: Typical Cross-section of Segment showing Bottom Flange and Web Rebar Details, Plan Sheet BO1-7

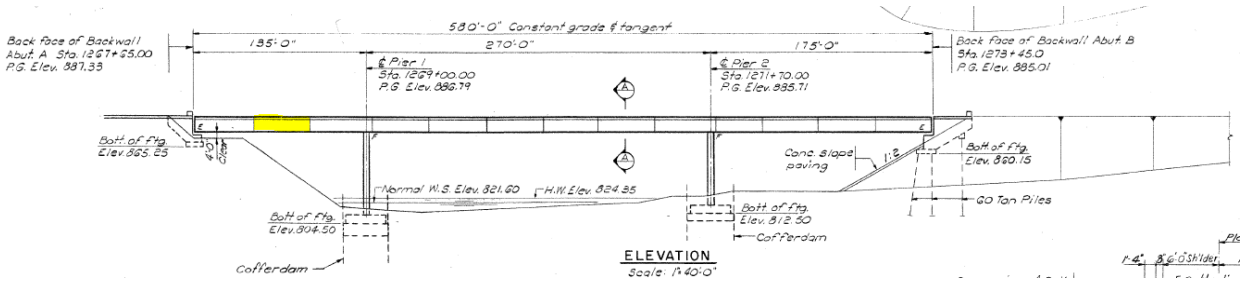

Figure 3.113: Segments arrangement showing location of segment 2 between abutment A and pier 1, Plan Sheet BO1-1

3.6.1.4 Ultrasonic Assessment on Web within Segment 2 along Longitudinal and Transverse Reinforcement to Check for Pockets of Voids

Ultrasonic assessments were conducted on grids set-out along the longitudinal and transverse reinforcement along the web in segment 2 to check for the presence of large pockets of voids and delamination around reinforcement. The grids were mapped out using US-131 plan sheet from Job Number 16246A, sheet B01-7 and the Ground Penetrating Radar. Ultrasonic assessment was performed at a standard frequency of 50 kHz, frequency. Three (3) runs of scanning were conducted at selected location for quality evaluation purposes. Scanning locations were determined mainly by visual inspection and assessment was done perpendicular to the cracking surface. Detail results and analysis are presented in Section 5.3.1.4 of this report.

3.6.1.5 Magnetic Flux Leakage Scanning on Selected Bottom Flange within Segment 2

A 39 ft – 6 in x 11 ft testing grid was established on the bottom flange within segment 2 of the US-131 Muskegon River Bridge. The grid was comprised of forty-nine transverse reinforcement spaced approximately ten inches and seventeen longitudinal reinforcement spaced approximately seven inches. All of the transverse reinforcement and the five labeled longitudinal reinforcement, shown in Figure 3.114 were each scanned three times with the prototype Magnetic Flux Leakage (MFL) mobile scanner. The dashed white longitudinal lines represent reinforcement that were not scanned due to time constraint. The transverse reinforcement, labeled from V1 to V49, were scanned from east to west and the longitudinal reinforcement, labeled HA-HE, were scanned from south to north.

An issue that was encountered was the unfinished, rough floor of the bottom flange. The MFL mobile scanner has a clearance of ¾ of an inch which was not enough to clear on an uneven surface. This was not an issue with previous testing of laboratory prepared and the Kent County salvaged beams since those beams had smooth surfaces. The testing team resolved this issue by using 1/8" wood strips, as shown in Figure 3.115 to aid in smooth run of the MFL mobile scanner. This allowed the MFL mobile scanner to scan each reinforcement unimpeded. Another issue that the team encountered was that the permanent magnets were collecting excess magnetic materials from the the floor. This could affect the scan data if the buildup around the magnets was not removed. It is recommended that prior to future field tests, the test area be swept using magnetic sweeper to

pick up the magnetic material before scanning. Detail results and analysis are shown in section 5.3.3 of this report.

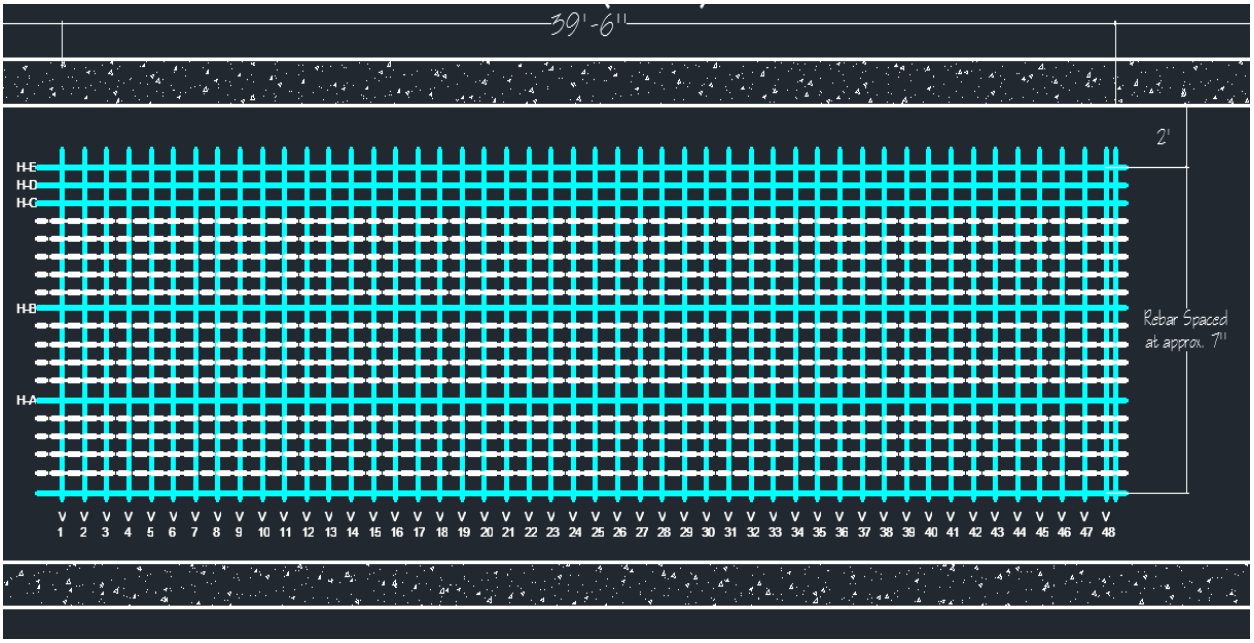

Figure 3.114: MFL Testing Grid Set-up within Bottom Flange of Segment 2

Figure 3.115: MFL Mobile Scanner with Temporary 1/8" Wood Strips

3.6.1.6 Electrochemical half-cell Assessment on Selected Web Segment within Segments 2 and 4.

Elcometer 331 half-cell meter was used to measure the corrosion potential on selected areas on the web of the southbound bridge within segments 2 and 4. Typical instrument configuration for the Elcometer 331 half-cell measurements is shown in Figure 3.118. The first test area within segment 4 had visible diagonal shear cracks which had been filled with epoxy. The second test area was about 20 ft from the north abutment within segment 2. The test areas are shown below on Figure 3.117 and 3.119

The reinforcement locations on the web were located with Ground Penetration Radar (GPR) and were mapped by chalk line as shown in Figure 3.116. The vertical bars were at about 7 inches spacing and the horizontal bars were at about 11 inches spacing. Reinforcement were exposed by hammer drill for each test area and the exposed reinforcement were connected to the half-cell meter. After water was sprayed on the test areas for better conductivity, data was collected from 50 intersection points of the vertical and horizontal bars in each test area. The data were collected three times and a total of about 150 data were collected from each test areas. Detail results and analysis are presented in section 5.3.2 of this report.

Figure 3.116: Locating Longitudinal and Transverse Reinforcement on web of Segment #2 Using Ground Penetrating Radar (GPR)

Figure 3.117: Electro-chemical half-cell Assessment of selected Section of Web along Segment 2

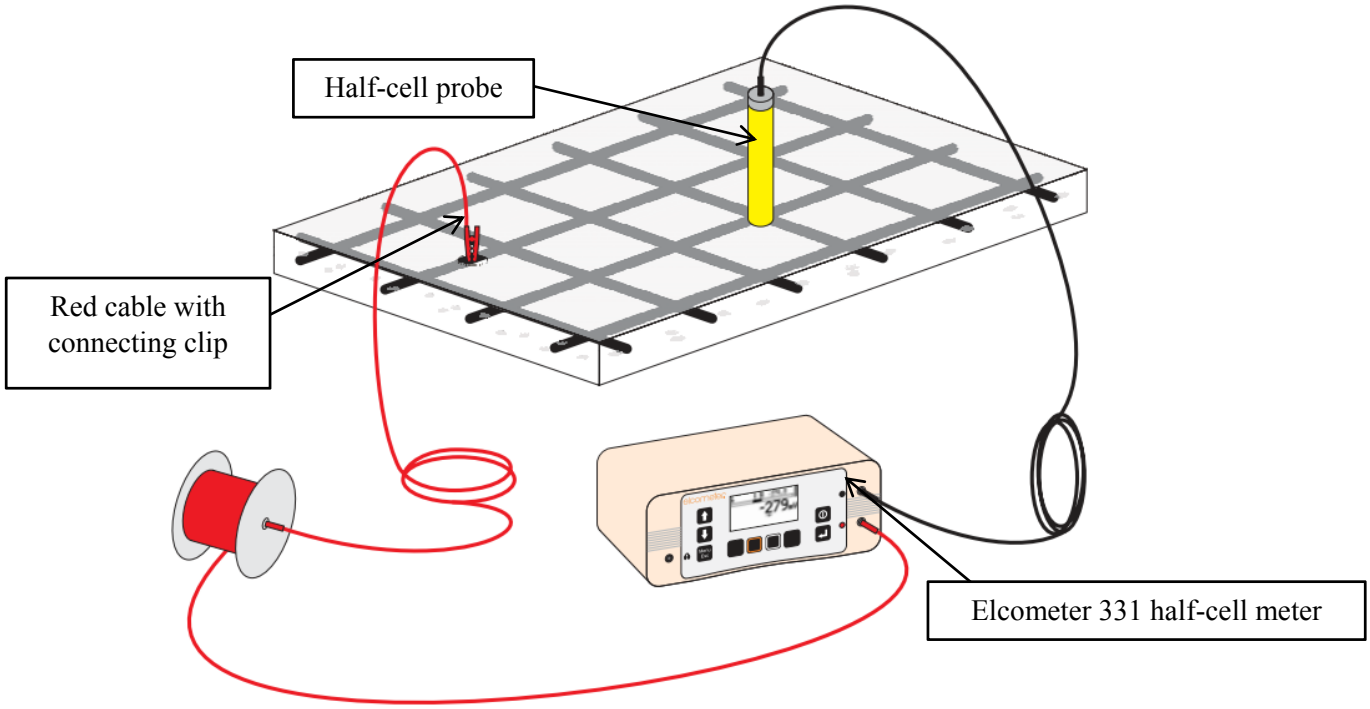

Figure 3.118: Typical instrument configuration for half-cell measurements (Half-cell meter operating instructions manual)

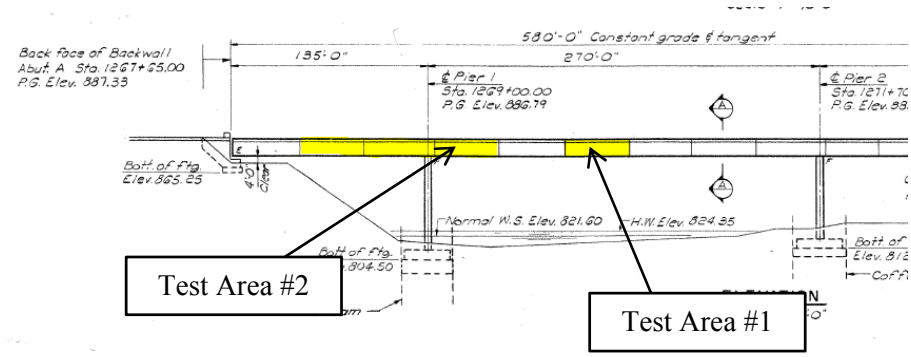

Figure 3.119: Layout of Southbound Bridge indicating Test Areas #1 and #2

3.6.2 Side-by-side Box Beam on I-96 over Canal Road, Lansing.

Field investigation was conducted on two (2) exterior box beams 3-A-8 and 3-M-11 along span #3 of Bridge S08 to check the thickness of the box beams web as well as to investigate on the probability of corrosion of the transverse reinforcement. This was necessitated as a result of excerpts from a consultant fabrication inspection report for bridge S08 that indicates that internal voids for some of the box beams had shifted during casting, as detailed in Table 4 of Research Report TI-2027, by Structural Research Unit of MDOT reported in June, 2004. Figure 3.120 shows I-96 over Canal Road in Lansing.

Figure 3.120: I-96 over Canal Road, Lansing

3.6.2.1 Ultrasonic Assessment on Web of External Box Beam on Span #3, Beam 3-M-11 on Bridge S08 using MIRA.

Ultrasonic assessment on the web of Beam 3-M-11 on Bridge S08 were conducted at a standard frequency of 50 kHz. Scans were done along the length of the box beam as shown in Figure 3.121. Scans were done three consecutive times along the length of the selected beam. Figure 3.122 shows a typical scan along web of box beam 3-M-11 with back-wall reflection indicating web thickness. Detail results and analysis are presented in section 5.2.1 of this report.

Figure 3.121: Scanning along web of Box beam 3-M-11

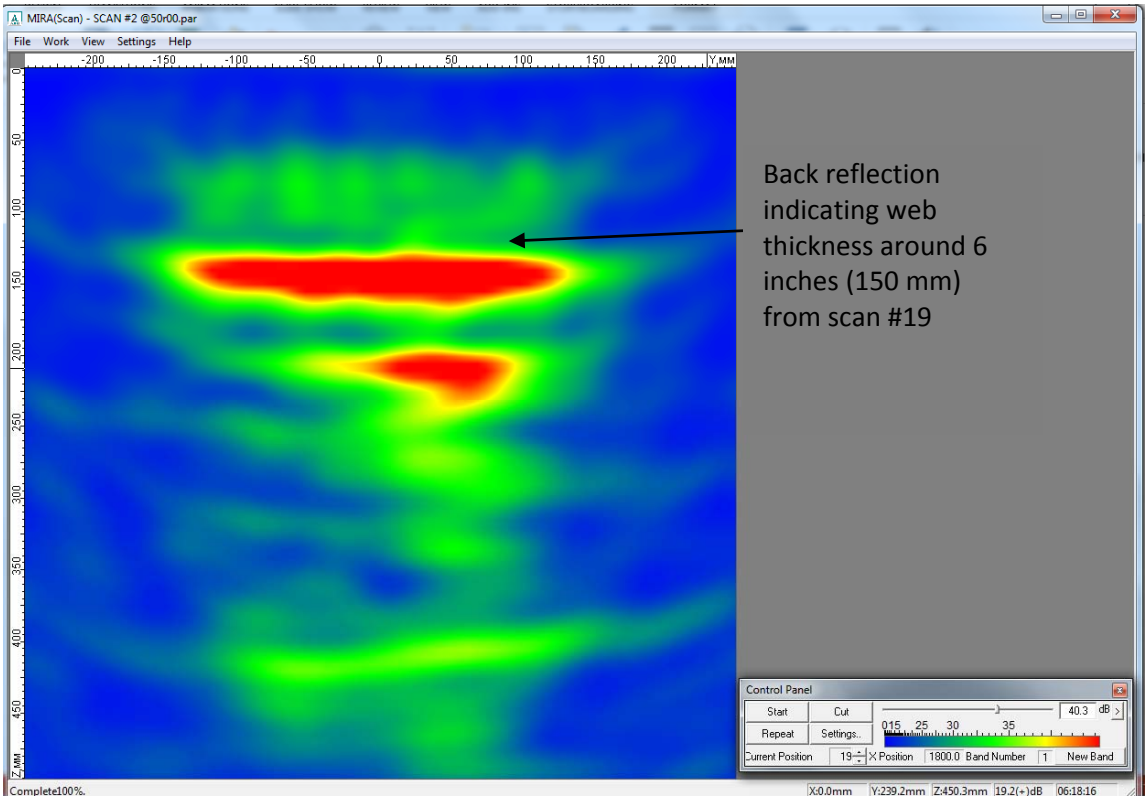

Figure 3.122: Typical scan along Web of box beam with back Reflection indicating Web thickness

3.6.2.2 Electro-chemical half-cell Assessment on Web of External Box Beam on Span #3, Beam 3-M-11 on Bridge S08, using Canin.

Canin was used to measure the corrosion potential on selected areas on the web of Box beam 3-M-11on span 3. Transverse reinforcement were initially located using reinforcement detector for connection to the canin as illustrated in Figure 3.123. Figure 3.124 depicts conducting electro-chemical analysis on the web of external beam 3-M-11. Detail results and analysis are presented in section 5.2.2 of this report.

Figure 3.123: Locating Transverse Reinforcement for Electro-chemical Assessment using Reinforcement Detector

Figure 3.124: Conducting Electro-chemical Analysis on the Web of External Beam 3-M-11.

CHAPTER 4: LABORATORY TEST RESULTS.

Results, detailed analysis and discussions of the laboratory investigation are presented in this chapter. Ultrasonic assessment as well as magnetic flux leakage assessment of the various laboratory specimens have been analyzed and detailed. Ultrasonic assessment using statistical matched pairs and comparison of scanned intensities of scans on defects as against scans without defects have been analyzed for Specimen 1 beams, (S1-1 and S1-2). Ultrasonic and magnetic flux leakage assessments analysis have been conducted for Specimen 2 beams (S2-1, S2-2 and S2-3). Assessment of grouting defects of simulated post-tensioned beams have also been analyzed for Specimen 3 beams (S3-1, S3-2, S3-3 and S3-4) using ultrasonic assessment. The following were details of laboratory evaluated specimen.

MDOT salvaged beams received from Kent County Road Commission as well as three sets of laboratory prepared specimen were evaluated in the laboratory. Two samples of Specimen 1 laboratory beams were constructed according to the geometry stipulated in MDOT Bridge Design Guides 6.65.10A with pre-induced defects to simulate voids created around prestressed strands and post tensioned cables as a result of corrosion by using plastic tubes. Three samples of Specimen 2 laboratory beams were constructed with pre-induced grinding defects covered with plastic tubes to simulate cross-sectional area loss for detection and quantification using ultrasonic assessment and magnetic flux leakage system. The third set of laboratory prepared specimen (Specimen 3) were made up of four beams constructed to simulate grouting defects normally associated with post-tensioned cables to investigate how these voids were detected using ultrasonic 3D tomography.

4.1 Overview of Laboratory Specimen and Testing Set-ups.

An overview of laboratory specimens as well as their testing set-ups have been presented in the following Figures 4.1 through 4.3.

(a) Specimen 1 Box Beams, S1-1 and S1-2.

(b) Scanning on the side of S1-1

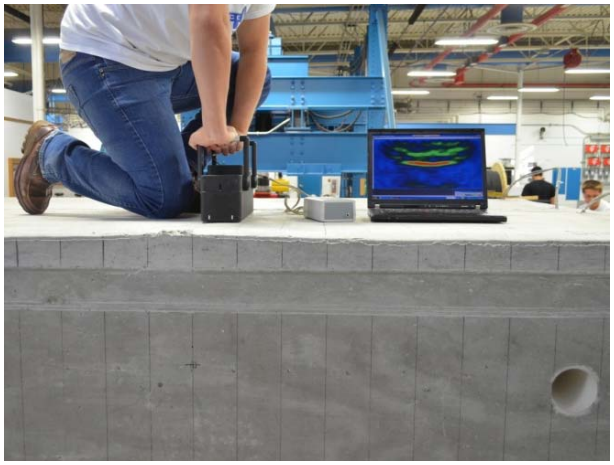

(c): Scanning on top of S1-2

(d): Scanning on the bottom of S1-2

Figure 4.1: Over view of Specimen 1 Testing Set-up

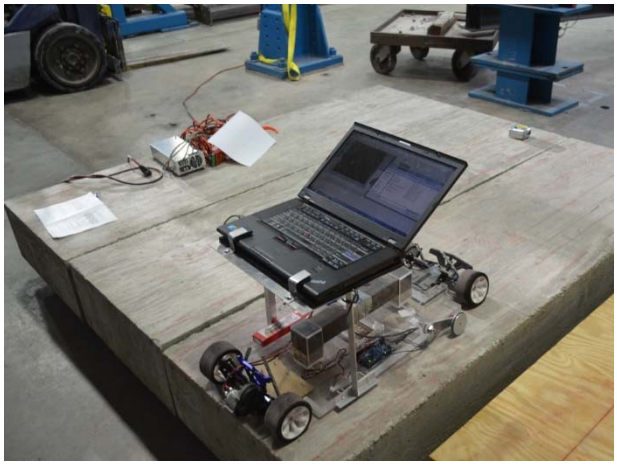

(a) MFL Mobile Scanner Setup

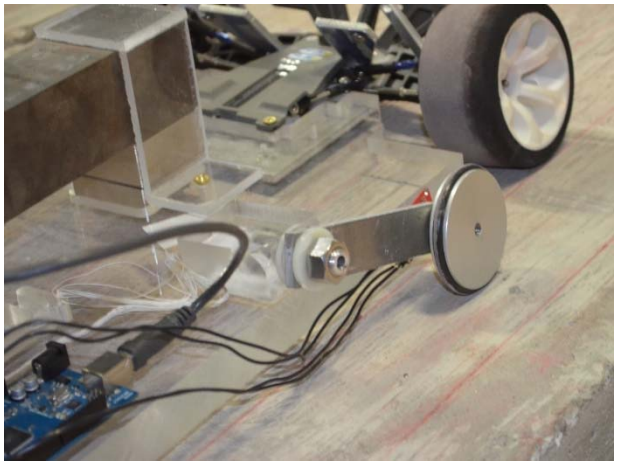

(b) Encoder for Distance Measurement

Figure 4.2: Over view of Specimen 2 Testing Set-up

(a): Scanning Top of S3-1

(b): Scanning Side of S3-1

(c): Scanning Top of S3-2

(d): Scanning Top of S3-3

Figure 4.3: Over view of Specimen 3 Testing Set-up

4.2 Analysis of Ultrasonic Assessment Data Using Statistical Matched Pairs

4.2.1 Laboratory Case study: S1-1 and S1-2 Box Beams

Ultrasonic assessment data from the various testing protocols for the laboratory beams have been analyzed using statistical matched pairs. The aim is to determine if there exists a statistically significant difference between the as built locations of the reinforcement and defects as compared to the diagnostic locations. The values of the measured parameters indicating the location of reinforcement and defects as detected by the ultrasonic assessment were recorded and labelled as diagnostic distances. Mean and standard deviation of the differences between the as built and diagnostic distances of the embedded reinforcement and defect as well as those of the field beams have been calculated using the computer software, Minitab 17.

The statement: H_0: $\mu_d = 0$, is called the null hypothesis. It states the equality of all arithmetic means difference between as built and diagnostic locations is equal to zero. The null hypothesis is tested against what is called the alternative hypothesis: H_1: $\mu_d \neq 0$, $\mu_i \neq \mu_j$ for at least one pair of $i \neq j$, the alternative hypothesis means there is a difference between the as built and diagnostic distances. To test this hypothesis, a procedure is implemented for taking random samples, computing an appropriate test statistics and then rejecting or accepting the null hypothesis H_0 based on the values found for the adopted test statistic parameter called the critical values. One way to report the results of a hypothesis test is to state that the null hypothesis is rejected or is not rejected at a specific value of significance level, α. The value of α represents the probability of rejecting H_0 while it is true, and therefore, $(1- \alpha)$ represents the probability of accepting the null hypothesis while it is true. (Martin and Krista, 2012).

As mentioned above, the comparison between the mean differences were based on statistical two-tailed test statistics. This test allows to determine if two independent data sets, normally distributed or with data sets greater than 30 are significantly different from each other. A confidence interval of 95% with significance level $\alpha = 0.05$ was used to assess the difference. All data sets with respect to distance measurements were undertaken in millimeters because the default readings from the ultrasonic equipment (MIRA) used were in millimeters. The conversion between millimeters and inches is 25.4 mm = 1 inch or 1 mm = 0.0393701 inch.

Figure 4.4 shows a typical cross-section of box beams (S1-1 and S1-2). A typical B-scan of laboratory full scale box beam S1-1, indicates that there is a 7 mm difference between the actual (as build) thickness of top flange and the diagnostic thickness of the top flange as detected by the ultrasonic equipment (MIRA) at a scanning frequency of 50 kHz and dB of 40 (see Figure 4.5). Typical scan results on stirrup without defect as against typical scan on those with defect are shown in Figures 4.6 and 4.7 as obtained at a scanning frequency of 80 kHz and dB of 35.

The testing protocols were executed as outlined below:

- Complete scan of all 4-longitudinal surfaces to verify concrete thickness
- Localized scan on reinforcement and strands without defect with varied frequencies of 30, 40, 50, 60, 70, 80, 90 and 100 kHz
- Localized scan on reinforcement and strands with defects each with varied frequencies of 30, 40, 50, 60, 70, 80, 90 and 100 kHz

A summary of statistical computations for beams S1-1 and S1-2 for the different testing cases have been tabulated in Tables 4.1, 4.2 and 4.3:

The goal was to get an appraisal of MIRA's ability to provide assessed scanned details to be compare with as built documented details. The default frequency of shear waves recommended for ultrasonic testing using MIRA is 50 kHz for normal testing (Reference: User Manual for MIRA Tomographer, August, 2009, Germann Instruments). However, for testing close to the surface, a higher frequency between the ranges of 70-100 kHz is employed to potentially capture reflections from smaller defects. For testing at deeper depths, a lower frequency is preferred. Ultrasonic assessment (MIRA) was not used to directly detect corrosion of embedded reinforcement and strands, but instead to detect typical deterioration of concrete such as delamination, cracking and spallings that follows the corrosion process.

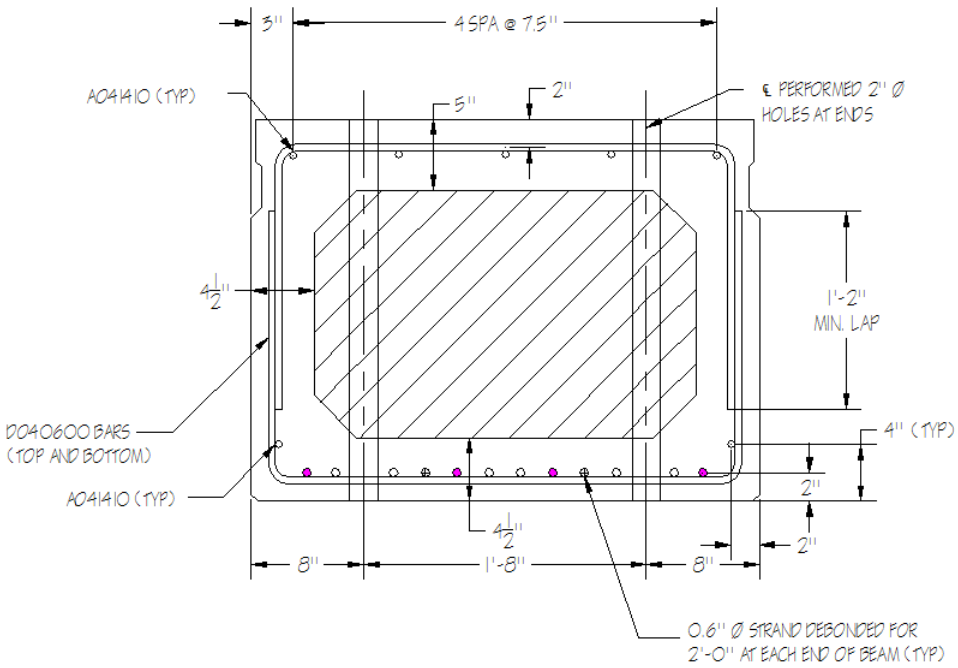

Figure 4.4: Typical cross-section of box beams (S1-1 and S1-2)

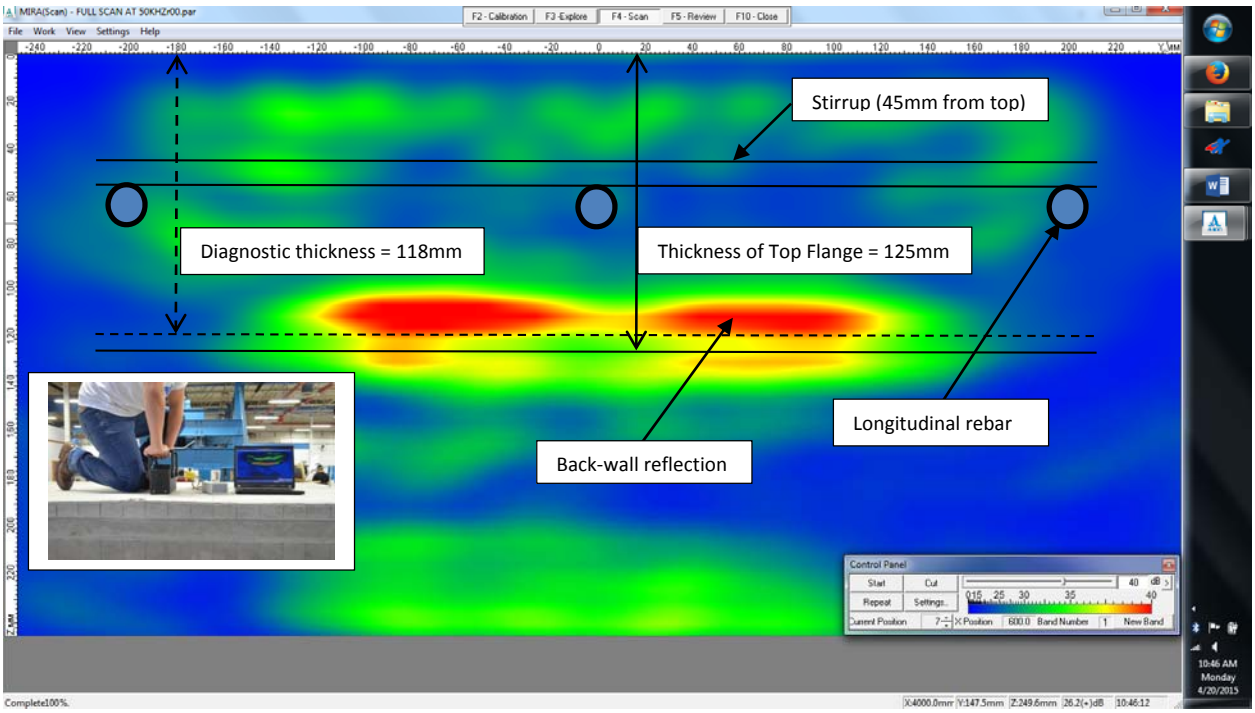

Figure 4.5: Typical scan indicating diagnostic and actual thickness of top flange of S1-1 between diaphragms with y-axis showing scan depth and x-axis indicating scan width at 50 kHz, 40 dB.

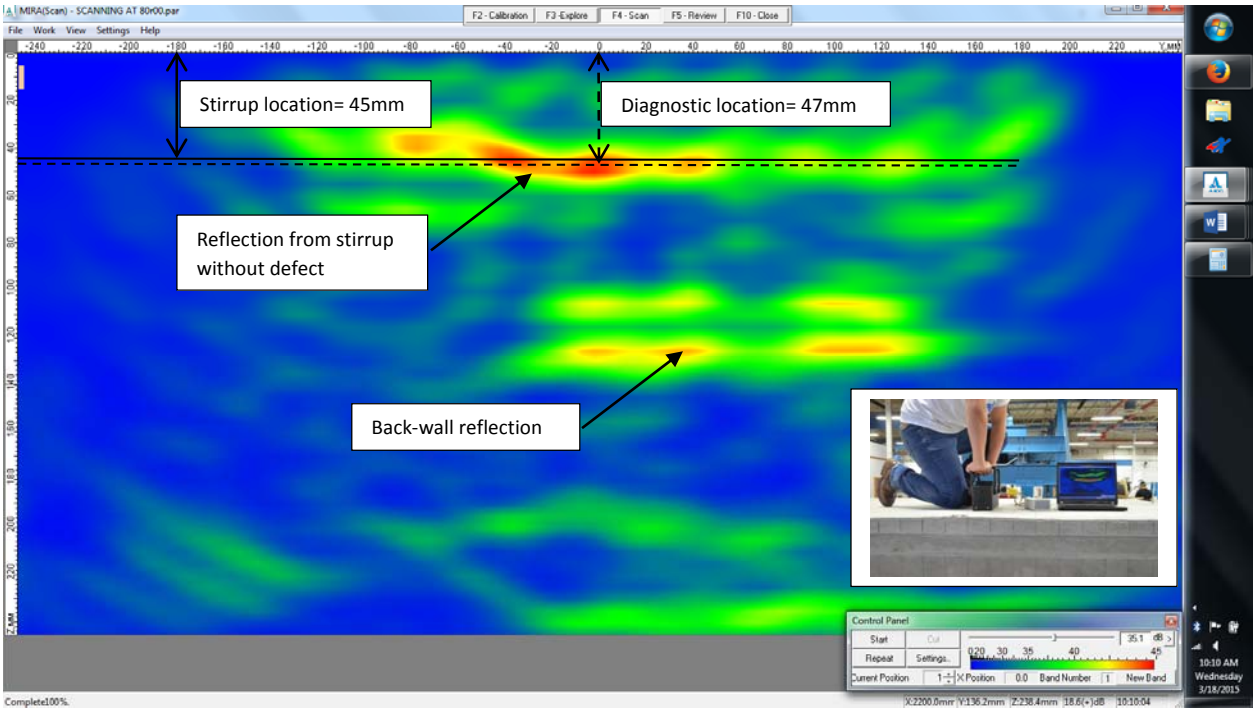

Figure 4.6: Typical scan on stirrup without defect of box beam S1-1 between diaphragms with y-axis showing scan depth and x-axis indicating scan width at 80 kHz, 35 dB.

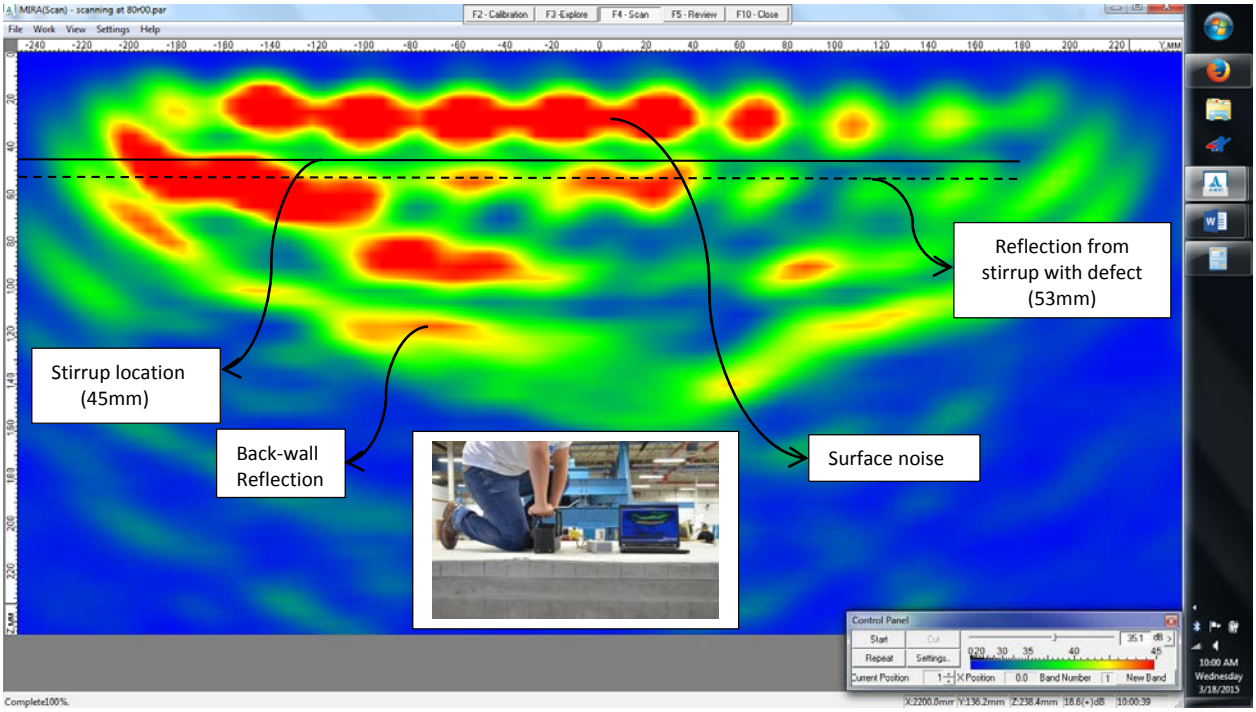

Figure 4.7: Typical scan on stirrup with defect (wrapped plastic tubes around rebar) of S1-1 with y-axis showing scan depth and x-axis indicating scan width at 80 kHz, 35 dB.

It is worth mentioning that in situations where scans have excessive surface and other multiple secondary reflections, the evaluating decibel (dB) can be reduced until surface and other secondary reflections reduces in intensity. This allow for the dominate reflection to be emphasized, especially when measuring at higher scanning frequencies. This technique was applied in Figure 4.6 to cause other reflections to reduce in intensity to enhance the reflections from stirrup and back-wall. Scan results along corroded strands and reinforcement tends to produce a lot of surface noise and other multiple reflections which tends to mere the actual reflections from corroded strands as well as the back-wall reflections especially at higher scanning frequencies. This is evident in Figure 4.7.

The reason for these issues is that the ultrasonic assessment as reported in the color contour maps is based on the principle that, the intensity of reflections are related to the magnitude of the change in material properties such as density and elastic modulus as shear waves propagates through the concrete materials. The rule of thumb for detecting delamination, cracking, spallings and other discontinuities is that, the size of the discontinuity must be greater than half of the scanning wave length to stand a reasonable chance of being detected. Using the relation: $\lambda = \frac{v}{f}$ where λ = wave length, v = velocity and f = frequency. Considering the selected scanning frequencies of 50, 80 and 100 kHz and considering a good concrete with an average shear wave velocity of 2500 ms^{-1}, a defect size should be greater than half of the wavelengths which are within the range of 1 inch (25 mm) for 50 kHz and 0.5 inch (12.55 mm) for 100 kHz to stand a reasonable chance of being detected.

Notation for matched pairs and Tables 4. 1 – 4.3

f = scanning frequency

α = significance level represents the probability of rejecting the null hypothesis

d = individual difference between two values in a single matched pair

μ_d = mean value of the difference d for the population of all matched pairs

$\overline{d}$ = mean value of the differences d for the paired sample data

s_d = standard deviation of the differences d for the paired sample data

t = test statistics

E = margin of error

CI = confidence interval

n = number of pairs of data

Hypothesis Test Statistic for matched pairs

$$t = \frac{\overline{d} - \mu_d}{\frac{s_d}{\sqrt{n}}}$$

Where degrees of freedom = n - 1

Confidence Intervals for Matched Pairs

$\overline{d} - E < \mu_d < \overline{d} + E$ Where Error of margin $E = t_{\alpha/2} \frac{s_d}{\sqrt{n}}$

Table 4.1: Checking concrete thickness of top & bottom flanges and side webs

Freq. (f) (kHz)	Significance Level (α)	Mean Difference $(\overline{d})$(mm)	Standard Deviation (s_d) (mm)	Test Statistic (t)	Margin of Error (E) (mm)	95% Confidence Interval (CI) (mm)
30	0.05	-4.286	1.652	-13.730	0.6406	-4.9266<μ<-3.6454
40	0.05	-1.464	2.426	-3.193	0.9408	-2.4048<μ<-0.5232
50	0.05	0.786	3.862	1.077	1.4984	-0.7124<μ<2.2844
60	0.05	1.643	4.356	1.996	1.6925	-0.0495<μ<3.3355
70	0.05	1.071	4.098	1.410	1.5558	-0.4848<μ<2.6268
80	0.05	1.357	4.778	1.503	1.8565	-0.4995<μ<3.2135
90	0.05	0.500	4.203	0.629	1.6330	-1.1330<μ<2.1330
100	0.05	0.638	2.478	1.386	0.9424	-0.3044<μ<1.5804

Considering critical value for n>30 but not equal to infinity, $t_{\alpha/2}$= ±2.048 (approximate)

The following explains the above table for estimating the concrete thicknesses for S1-1 and S1-2. Frequencies of 50, 60, 70, 80, 90 and 100 kHz showed there were not much differences between as built and diagnostic thicknesses of the top flange, bottom flange and the two side webs with test statistic values ranging from 0.629 to 1.966 which were all within critical range of ± 2.048 with a sample size of n>30 at a significance level 0.05 considering a scanning dB of 40. However, frequencies of 30 and 40 kHz showed there were some differences between actual and diagnostic thicknesses with test statistic values ranging from -3.193 to -13.730 which were outside critical range of ± 2.048, nevertheless at a significance level of α = 0.05 the calculated confidence intervals were all within a confidence range of -4.9266< μ_d < -0.5232. It can therefore be deduced from results of Table 4.1 that, using the ultrasonic assessment as a means of thickness measurement on

concrete specimen where it is difficult to take direct measurement with conventional measuring system, ultrasonic assessment can reliable measure concrete thickness with 95% certainty at scanning frequencies of 50 – 100 kHz. However, due to the fact that higher frequencies tends to pick very small details such as cracks, scanning frequencies should be restricted from 50 kHz to about 70 kHz for easy interpretation of scan results, when it comes to using the ultrasonic assessment as a means of checking concrete thickness in the range of approximately 2 inches (50 mm) to 1 foot (300 mm).

Table 4.2: Localized scan on reinforcement and strands without defect.

Freq. (f) (kHz)	Significance Level (α)	Mean Difference $(\overline{d})$(mm)	Standard Deviation (s_d) (mm)	Test Statistic (t)	Margin of Error (E) (mm)	95% Confidence Interval (CI) (mm)
30	0.05	1.867	4.531	2.250	1.6942	0.1728<μ<3.5012
40	0.05	2.931	4.834	3.265	1.8384	1.0926<μ<4.7694
50	0.05	-5.077	5.999	-6.102	1.7038	-6.781<μ<-3.373
60	0.05	-6.250	4.980	-8.333	1.5360	-7.786<μ<4.714
70	0.05	-7.920	5.96	-6.644	2.4555	-10.376<μ<-5.465
80	0.05	-5.042	4.175	-5.917	1.7632	-6.805<μ<-3.279
90	0.05	-9.520	3.441	-13.833	1.4204	-10.9404<μ<-8.099
100	0.05	-4.926	4.614	-4.926	1.9954	-6.7300<μ<-2.744

Considering critical value for n>30 but not equal to infinity, $t_{\alpha/2}$= ±2.048 (approximate)

The following can be deduced from Table 4.2 showing localized scan on rebar sizes #3 and 5/8 (7-wire) strand at depth of 50 mm within 125 mm thick flange. Frequencies of 30, 40, 50, 60, 70, 80, 90 and 100 kHz showed there were some differences between as built and diagnostic locations of rebar with test statistic values ranging from -13.833 to 3.2656 which were outside critical range of ± 2.048, nonetheless at a significance level of α = 0.05 the calculated confidence intervals were all within a confidence range of -10.9404< μ_d < 4.7694. It can be inferred from Table 4.2 that considering a 95% confidence interval, localized scans on reinforcement and strands have an accuracy of locating embedded steel reinforcement within a maximum confidence interval difference of ±4.9 mm when the concrete cover is 50 mm. This can be clearly seen from column 7 of Table 4.2 for all scanning frequencies, with the exception of 60 kHz which had a confidence interval difference of 12.5 mm.

Table 4.3: Localized scan on defects

Freq. (f) (kHz)	Significance Level (α)	Mean Difference $(\overline{d})$(mm)	Standard Deviation (s_d) (mm)	Test Statistic (t)	Margin of Error (E) (mm)	95% Confidence Interval (CI) (mm)
30	0.05	-1.480	2.663	-2.779	1.0993	-2.5793<μ<-0.3807
40	0.05	-4.600	4.583	-5.498	0.7784	-6.3136<μ<-2.8864
50	0.05	-7.933	4.653	-10.188	1.7397	-9.6727<μ<-6.1933
60	0.05	-8.968	2.415	-20.675	0.8832	-9.8512<μ<-8.0848
70	0.05	-7.310	2.740	-14.367	1.042	-8.352<μ<-6.268
80	0.05	-8.692	2.526	-17.549	1.0203	-9.7123<μ<-7.6716
90	0.05	-4.379	2.718	-8.676	1.0336	-5.4126<μ<-3.3454
100	0.05	-3.483	2.558	-7.333	0.9728	-4.4556<μ<-2.5102

Considering critical value for n>30 but not equal to infinity, $t_{\alpha/2}$= ±2.048 (approximate)

Results of localized scan on defect at depth of about 45mm within the 125 mm thick top flange using frequencies of 30, 40, 50, 60, 70, 80, 90 and 100 kHz showed there were some differences between as built and diagnostic locations of defects. This is deduced from Table 4.3 that shows test statistic values ranging from -20.575 to -2.779 which is outside the critical range of ± 2.048. However, at a significance level of α = 0.05 the calculated confidence intervals were all within a confidence range of -9.8512< μ_d < -0.3807. It can be inferred from Table 4.3 that considering a 95% confidence interval, localized scans on defects have an accuracy of locating defects within a maximum confidence interval difference of ±3.47 mm within concrete with concrete cover of about 45 mm. This can be clearly seen from column 7 of Table 4.3 for all scanning frequencies.

Considering the above analysis it is evident that the ultrasonic assessment using the 3D tomography is able to estimate the thickness of concrete specimen with adequate accuracy. It can be used in situations where it is difficult to use the traditional method of measurement for example when checking the thickness of a concrete specimen which can only be assess from one side.

4.3 Analysis of Ultrasonic Assessment Data Using Comparison of Reflected Intensities

4.3.1 Laboratory Case Study: S1-1 and S1-2 Box Beams

Figure 4.8 shows simulation of defects along reinforcement for box beams S1-1 and S1-2 with defect locations documented before placing of concrete. A side-by-side comparison of scans at 35 dB at a frequency of 80 kHz on reinforcement and strands with defects as against those without

defect showed there were significant differences in scanned intensities. Detail comparison have been shown by comparing scanned intensities for Figure 4.9 (a) (b) (c) showing localized scans from defects as against those of Figure 4.10 (a) (b) (c) showing scans from reinforcement and strands without defects.

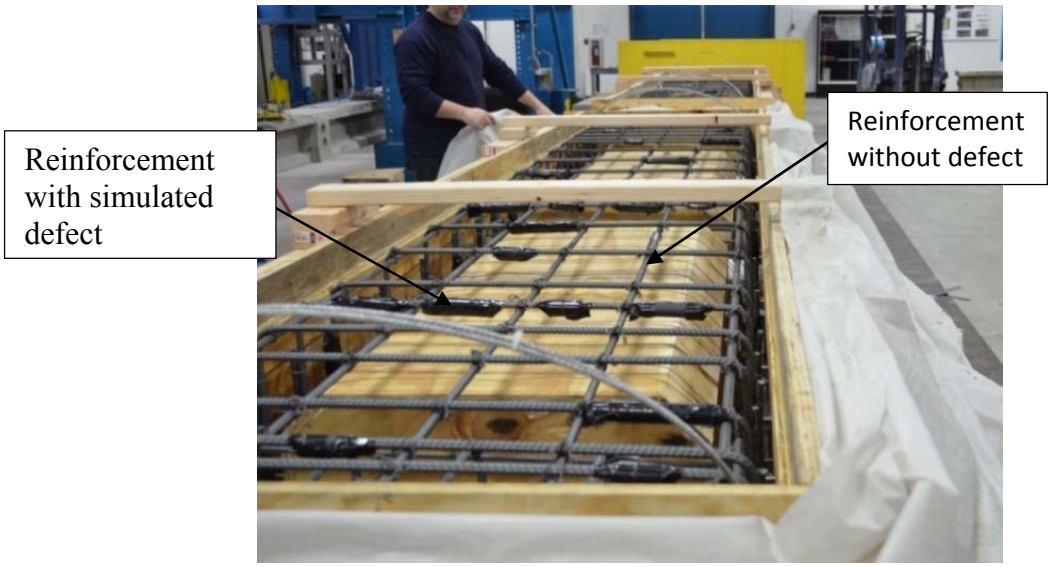

Figure 4.8: Reinforcement cage set-up showing rebar with and without defects

Detailed comparison of Figures 4.9 and 4.10 clearly show that due to the voids around the steel reinforcement in the case of Figure 4.9, the intensity of the reflections are higher compared to those of Figure 4.10. This is what is anticipated considering the under-lining principle of the ultrasonic assessment. The simulated defects had lengths of 50, 100, and 150 mm (2, 4 and 6”). The rule of thumb for detecting delamination, cracking, spallings and other discontinuities is that, the size of the discontinuity must be greater than half of the scanning wave length to stand a reasonable chance of being detected.

Considering the selected scanning frequencies of 30 – 100 kHz and considering a good concrete with an average shear wave velocity of 2500 ms^{-1}, a defect size should be within the range of 1.68 inch (42 mm) for 30 kHz and 0.5 inch (12.5 mm) for 100 kHz to stand a reasonable chance of being detected. The following color code have been selected for presentation to explain the subsequent figures for comparison of scans on defects as against scans without defects.

No change in shear wave reflection

Medium change in shear wave reflection

High change in shear wave reflection

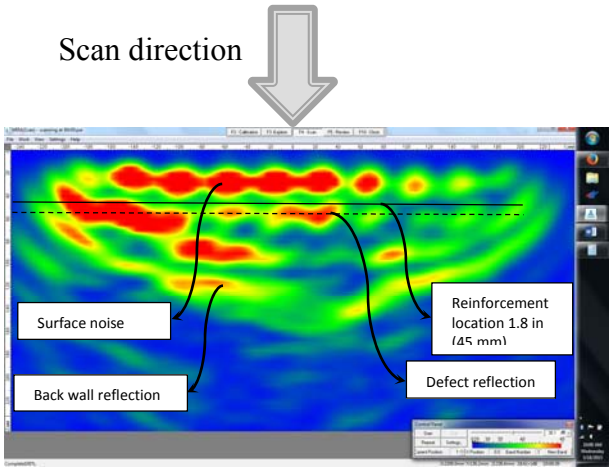

Fig. 4.9(a):scan on reinforcement with defect

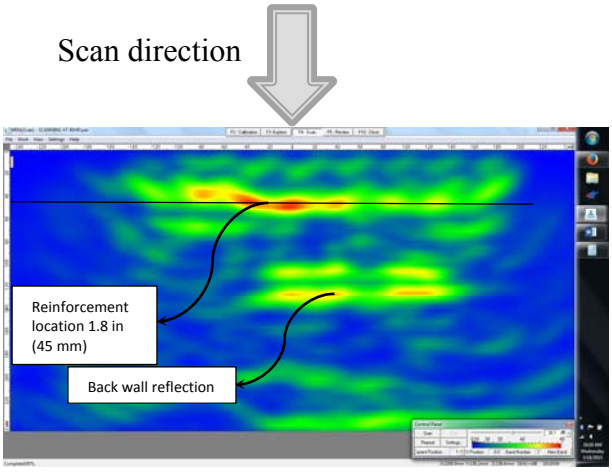

Fig. 4.10(a):scan on reinforcement without defect

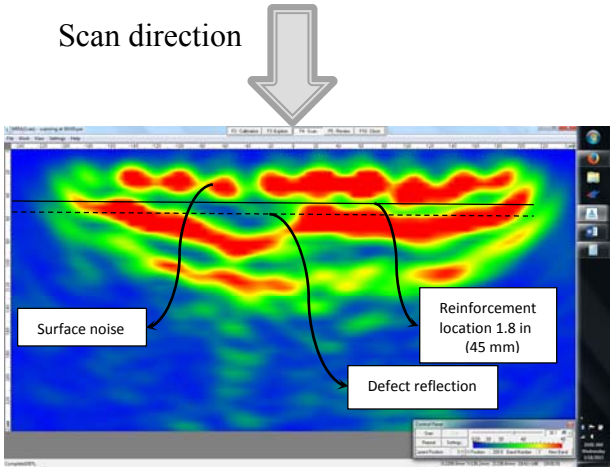

Fig. 4.9(b):scan on reinforcement with defect

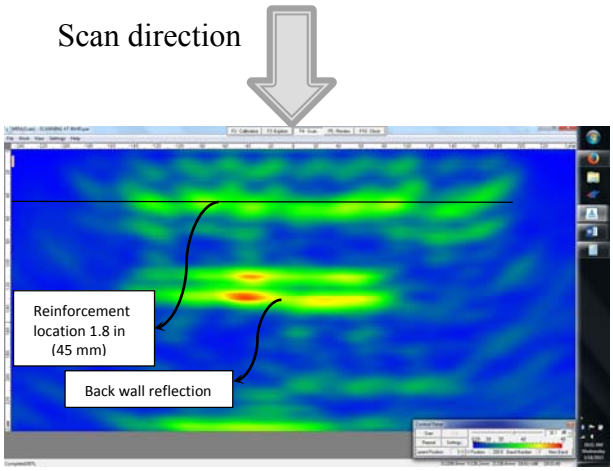

Fig. 4.10(b):scan on reinforcement without defect

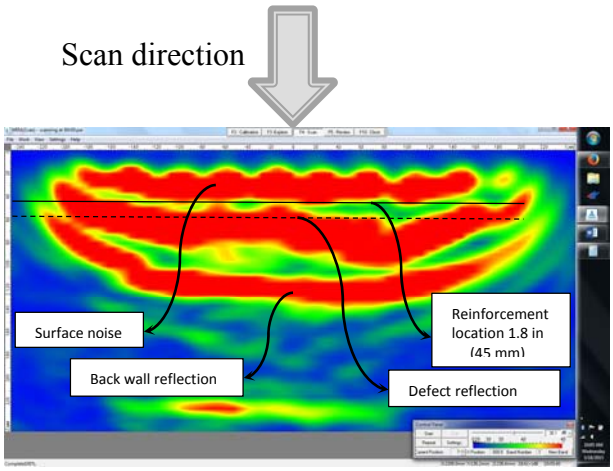

Fig. 4.9(c):scan on reinforcement with defect

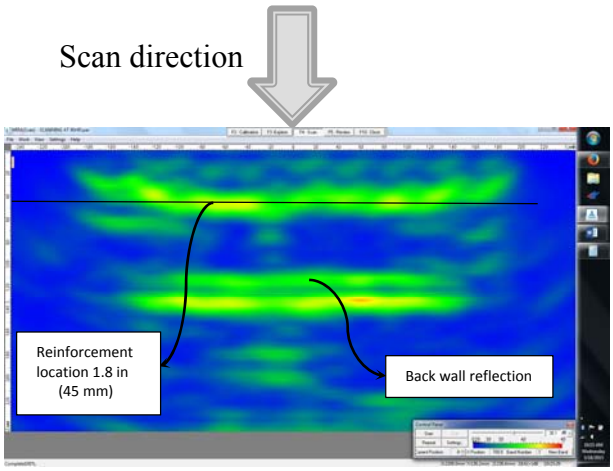

Fig. 4.10(c):scan on reinforcement without defect

4.3.2 Laboratory Case Study: S2-1, S2-2 and S2-3 Beams

Specimen 2 had two beams S2-1 and S2-2 simulated with various cross-sectional area losses ranging from 5% - 30% along various reinforcement lengths used as top and bottom reinforcement. A third beam S2-3 had 5/8 (7-wire) steel strands simulated with different lengths of wire cuts ranging from 6 mm to 25 mm (0.25 to 1") as well as different number of wire cuts ranging from a single wire cut to four (4) wire cuts. The essence of the above was to simulate the effect of corrosion on reinforcement and strands embedded in concrete which are usually associated with cross-sectional area losses.

Comparably, scans at frequencies varying from 50 to 90 kHz reviewed at 40 decibel (dB) on reinforcement and strands with defects as against reinforcement and strands without defect for the case of specimen 2 beams also showed there were differences in scans intensity. Details in Figure 4.12 (a) and (b) show localized scans from defects and Figure 4.13 (a) and (b) show scans from reinforcement and strands without defects. Figure 4.11 shows reinforcement cage set-up showing simulation of defects on reinforcement and strands. Comparison of figures 4.12 and 4.13 clearly show that due to the voids around the reinforcement in the case of figure 4.12, the intensity of the reflections are higher compared to those of figure 4.13. This is due to the fact that as the shear waves travel from the concrete medium through the voids simulated around the reinforcement and strands as shown in Figure 4.11 there are reflections due to differences in density and elastic properties between the different materials. Hence part of the shear waves are reflected back to the transducers for interpretation as reflection showing the location of the voids while the remaining shear waves travel through the entire concrete specimen. As the shear waves move out of the concrete sample to the surrounding air, the remaining un-reflected shear waves are also reflected back to the transduces and interpreted as back wall reflection which indicates the thickness of the concrete beams.

The results from scanning frequencies of 80 kHz and 90 kHz were selected due to the proximity of the reinforcement and strands to the scanning surface of the concrete and considering the fact that lower scan frequencies do not give clear distinction between scans on reinforcement and strands with near surface defect as against those without defects. This is what was expected

considering the fundamental principle behind ultrasonic testing that higher scan frequencies have lower wave lengths which tends to pick smaller details compared to lower scan frequencies.

(a) S2-2 with cross-sectional area loss

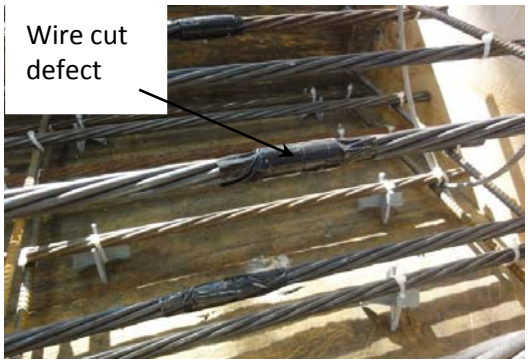

(b) S2-3 showing strands with wire cuts

Figure 4.11: Reinforcement cages set-up for S2-2 & S2-3 (Refer to Figures 3.32-3.36 for details)

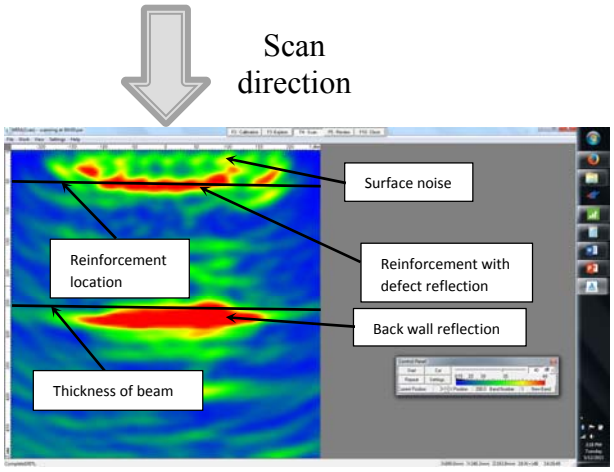

Figure. 4.12(a): scan on reinforcement with defect, 80 kHz

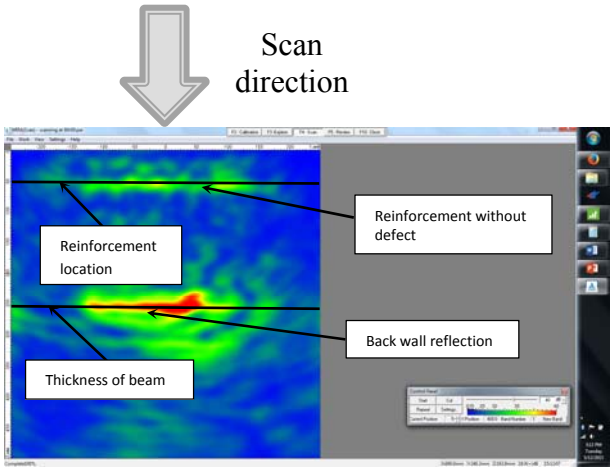

Figure. 4.13(a): scan on reinforcement without defect, 80 kHz

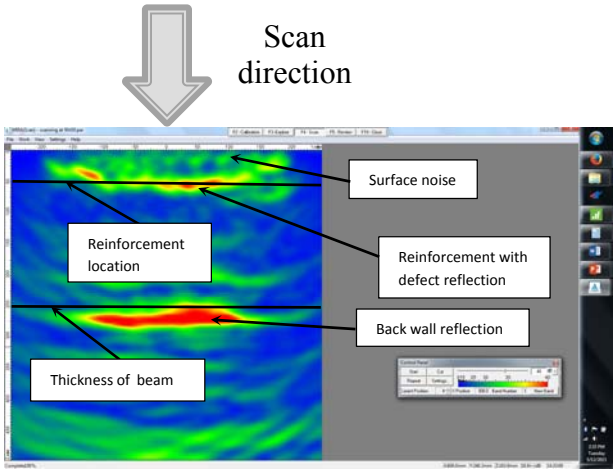

Figure. 4.12 (b): scan on reinforcement with defect, 90 kHz

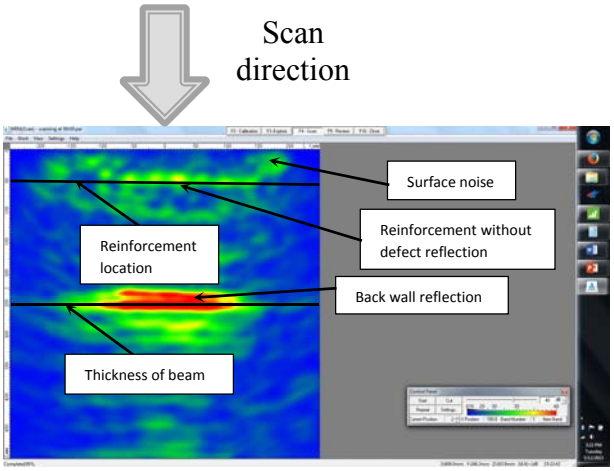

Figure. 4.13 (b): scan on reinforcement without defect, 90 kHz

4.3.3 Laboratory Case Study for Grouting Defects of S3-1, S3-2, S3-3 and S3-4

Results of ultrasonic assessment of grouting defects in laboratory simulated post-tensioned beams are discussed in this section. The objective was to verify the efficacy of ultrasonic assessment using MIRA to assess beams induced with grouting defects to ascertain if these defects would be detected. Grouting defects which results in voids around strands in embedded ducts in post-tensioned beams give rise to problems such as possible ingression of moisture which causes corrosion and lack of redistribution of stresses within post-tensioned beams which in most cases results in catastrophic failure of these structures. The principal problem with post-tensioned beams is corrosion of tendons due to grouting problems during construction of these structures.

A side-by-side comparison of scans at 40 decibel (dB) of frequencies 50 and 60 kHz of test grids set along the post-tensioned profiles of the laboratory simulated beams is presented below. As detailed in the experimental section of this report, grouting defect evaluation were conducted on four (Specimen 3) beams with the following grouting defect simulations. Polyethylene corrugated draped duct was used to simulate tendon paths in positive and negative moment regions and grout was pumped in to consider grout defects such as insufficient grout coverage at angle breaks for S3-1. The same duct material with similar configuration as used for S3-1 was filled partially with water to check if the grout completely displaced the water in the case of S3-2. Grout mixed with polystyrene (defects) was pumped into straight steel duct to assess how the ultrasonic assessment could detect these defects for S3-3. S3-4 with steel duct was grouted vertically to ensure the duct was fully grouted to be used as a control for assessing grouting conditions of S3-1, S3-2 and S3-3. Ultrasonic testing was conducted on the four laboratory simulated beam before and after grouting.

Detailed comparison of Figures E-1 through E-10 (reference to Appendix E) presenting series of scans taken before and after grouting from S3-1, S3-2, S3-3 and S3-4 clearly show differences in scan intensities. The intensity of reflections are higher in the case of scans taken before grouting compared to those taken after grouting. This is due to the principle behind the ultrasonic assessment of concrete specimen where the intensity of reflections are related to magnitude of change in material properties such as density and elastic modulus as shear waves propagate

through concrete specimen. Due to the open post-tensioned ducts before grouting, scans taken before grouting have higher scan intensities irrespective of duct material used.

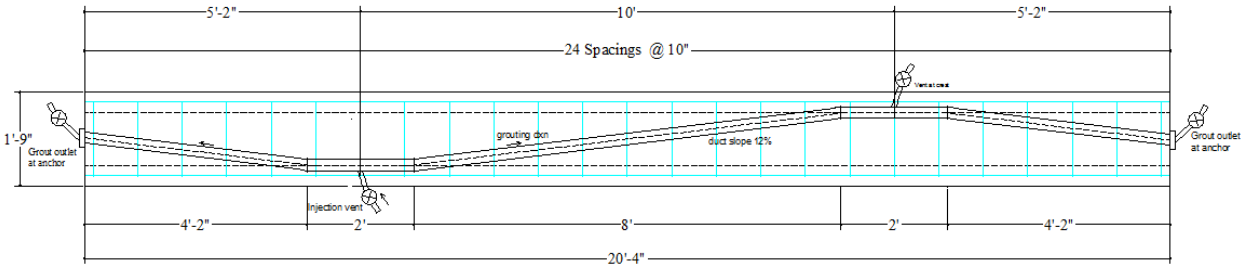

Figure 4.14: Configuration of S3-1 showing draped post-tensioned duct

Figure 4.15: Beam S3-1, showing draped post-tensioned duct

4.4 Analysis of MFL Data.

4.4.1 Background

When a magnetic yoke is passed over a magnetic material, like reinforcement steel, the magnetic field passing from the north to the south pole of the magnet is channeled through the steel. The density of this magnetic field remains constant if both the magnetic material volume and the distance from the yoke to the magnetic material are constant. The magnetic field creates an electrical current and the resulting voltage can be measured. The voltage is denoted the Hall Voltage and Hall Sensors are used to measure the Hall Voltage as shown in Figure 4.16. When a change occur in either the magnetic material volume or the distance between the yoke and the magnetic material; the Hall Voltage also changes. In this field investigation this phenomena is utilized to detect changes of magnetic prestressing strands. The term magnetic flux leakage refers to the condition where the magnetic material volume decreases resulting in an increased magnetic saturation of the remaining steel and hence the magnetic flux density lines 'leak'. This phenomena is depicted in Figure 4.16.

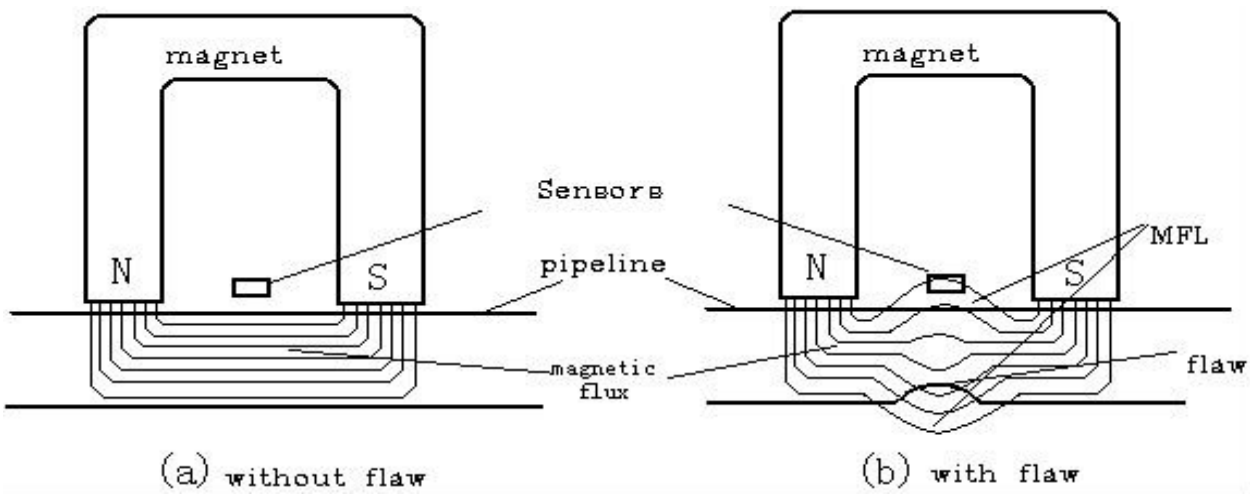

Figure 4.16. Depiction of magnetic flux density lines around magnetic member with or without cross sectional area reduction (ndt.net).

The Magnetic Flux Leakage system used in this study was developed at Lawrence Technological University. A reference manual have been developed for the MFL system. The strong earth magnet is mounted on a non-magnetic plate. Two sets of wheels and axles are mounted on the plate. Data

is collected as the magnetic flux leakage (MFL) vehicle is passing along the concrete surface. Hall Voltage is collected from ten Hall Effect sensors, the distance traversed is measured by a rotary encoder, and the data acquisition system time stamps the data. Data are collected and stored approximately every 1 to 2 inches. An example of the variation of hall voltage as it passes over an area of cross sectional loss is shown in Figure 4.17. Two sets of data are shown in Figure 4.17 for a vertical and a horizontal placed hall sensor. Since the effect of concrete on magnetic field is negligible, the field leakage may be detected by sensors in the air near the surface of the concrete. If the magnetic source and sensors are moved along the length of the concrete member, the changes in the field, due to the presence of flaws in steel, can be recorded as continuous in terms of time and the field amplitude. This is then analyzed to obtain information relevant to the location and extent of the flaw in the steel (Ghorbanpoor, 1999).

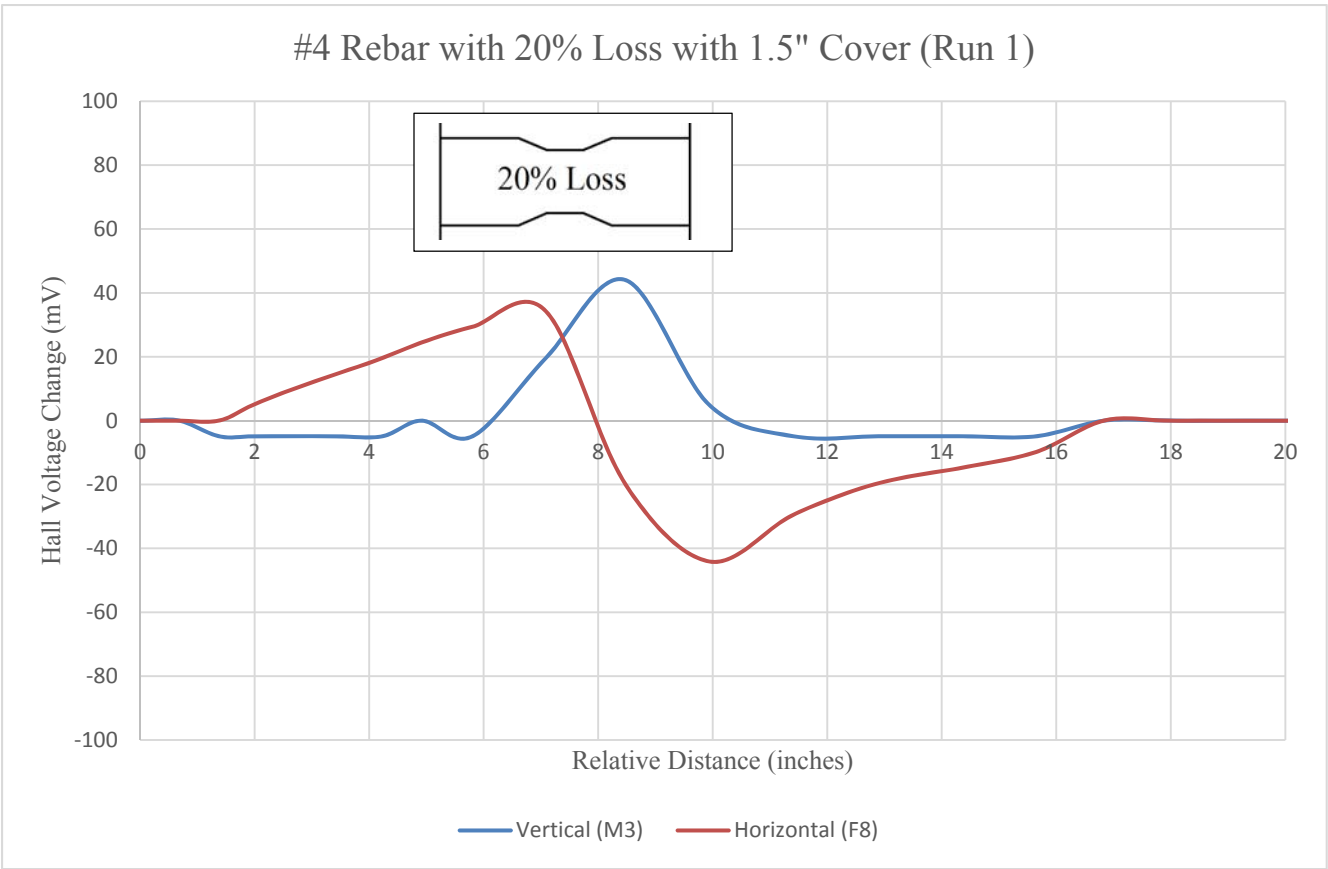

Figure 4.17. Variation in hall voltage output for area with or without cross sectional area reduction.

The system was calibrated using laboratory reinforced concrete beams with reinforcement simulating different cross-sectional area losses. The variables considered were reinforcement size, rebar depth, localized loss of rebar material, and localized loss of strand material. For more details refer to Section 3.3.1 of Chapter 3. The relationship between Hall Voltage and reinforcement cross sectional area for a reinforcement depth of 1.5 inches is shown in Figure 4.18 representing the vertical sensor (M3) in Figure 4.17. The rebar depth is the distance from the concrete surface to the center of the reinforcement. The relationship exhibits a stronger R^2 value for the parabolic than the linear relationship. The cross-sectional area loss is predicted for specimen 2 beams (S2-1, S2-2 and S2-3) by using the relationship between Hall Voltage (V) given as y and cross section area (in^2) given as x, and regression parameters a, b and c:

$$y = ax^2 + bx + c \tag{4.1}$$

$$Hall\ Voltage\ (V) = 0.0263x^2 - 0.1976x + 2.9222$$

The cross-sectional area can be estimated using the relative change in Hall Voltage.

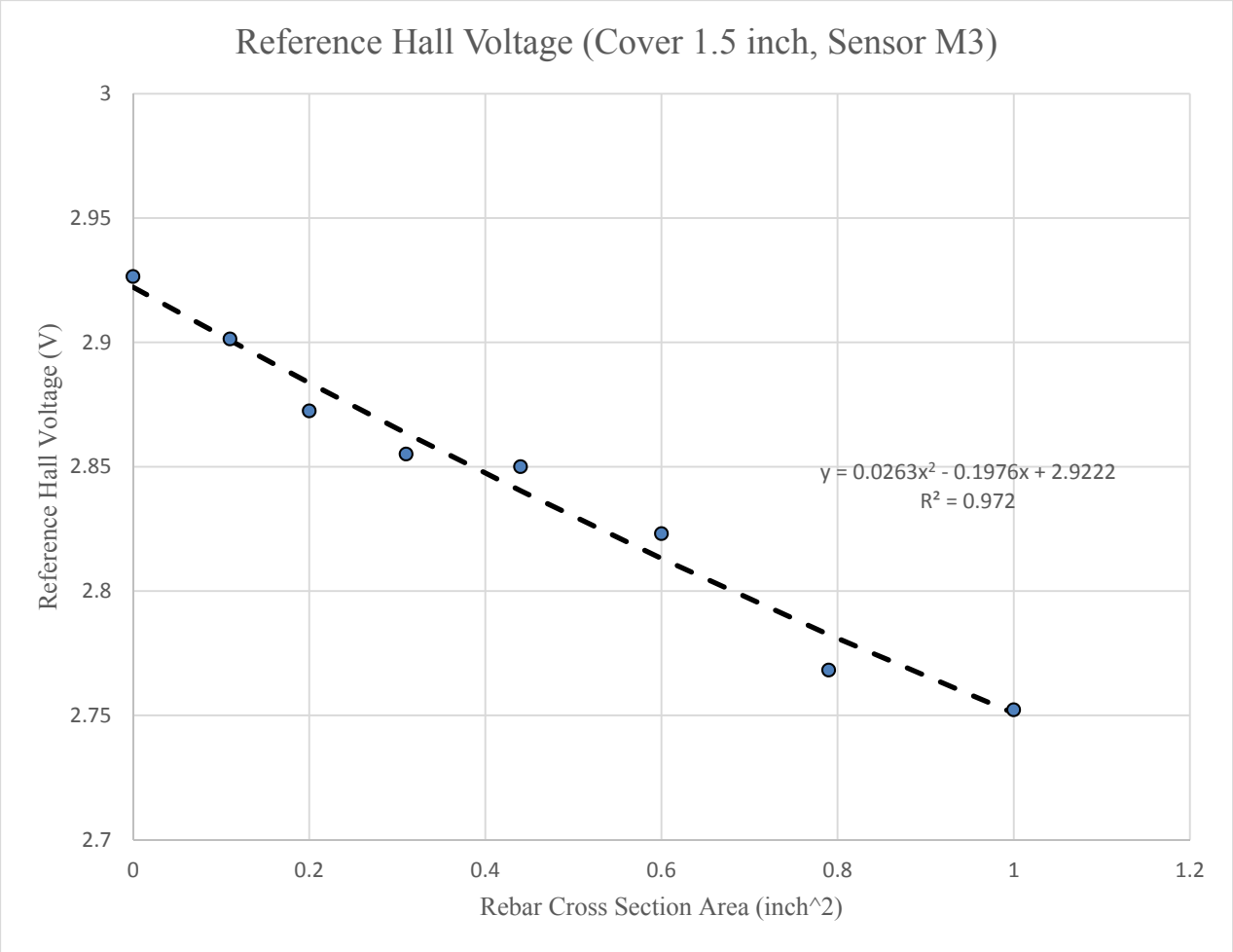

Figure 4.18. Relationship between hall voltage and cross sectional area of reinforcement for concrete cover of 1.5 inches.

The relationships between predicted and actual cross sectional area loss over a 12 inch length of a reinforcement are shown in Figure 4.19 for steel stirrup spacing of 9.5 and 19 inches, respectively. In both cases the reinforcement depth is 1.5 inches. There is excellent agreement between predicted and actual cross sectional area loss for S2-2 with stirrup spacing of 9.5 inches. There is adequate agreement for the case of S2-1 with stirrup spacing of 19 inches. The slopes of the linear prediction curves are very similar ranging from 0.78 to 0.82. The offset is, however, different between the two sets of data with 4% and 16% overestimation at 0% loss, respectively.

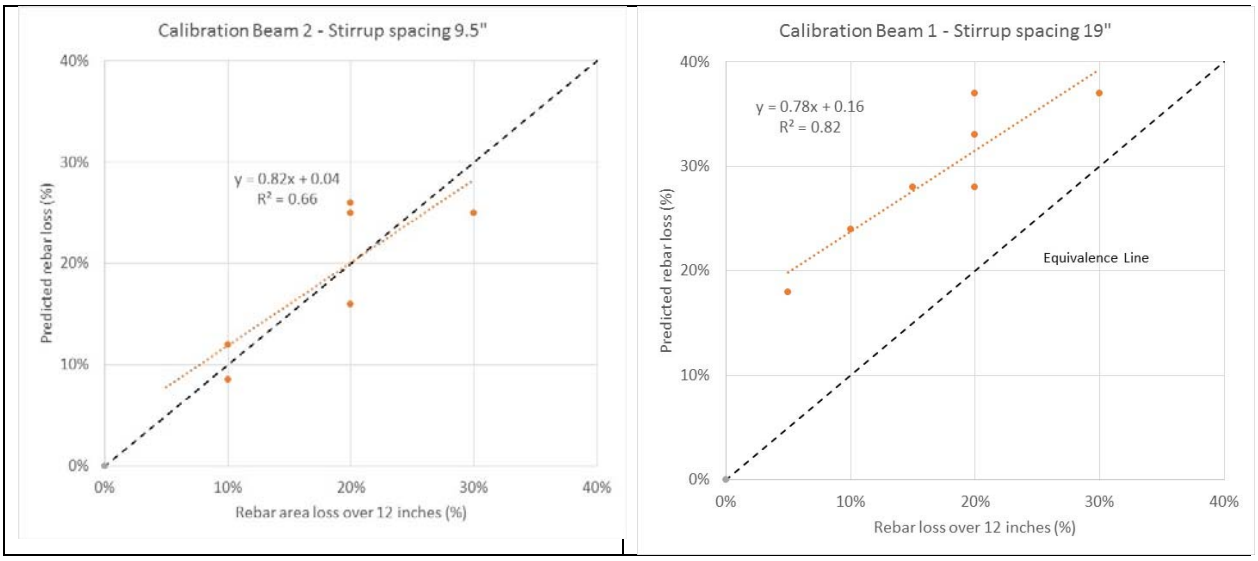

Figure 4.19. Predicted reinforcement cross sectional area loss versus actual reinforcement cross sectional area loss over 12 inches in calibration beams.

4.4.2 Laboratory Case Study: S2-1, S2-2 AND S2-3 Beams.

Results of recorded signals for sensor M3 along reinforcement and strands for a series of runs along each of the evaluated specimen 2 beams (S2-1, S2-2 and S2-3) are presented in this section. Signals from sensor M3 along each of the evaluated reinforcement and strands were superimposed to have a combined effect of signal profile. An average signal amplitude between stirrups without defect were imposed on the original M3 data for each of the runs to normalize the effects of stirrups and other embedded artifacts. Figures 4.21 and 4.22 show graphs for M3 consolidated and M3 adjusted for S2-1 rebar B with location of stirrups and cross-sectional losses.

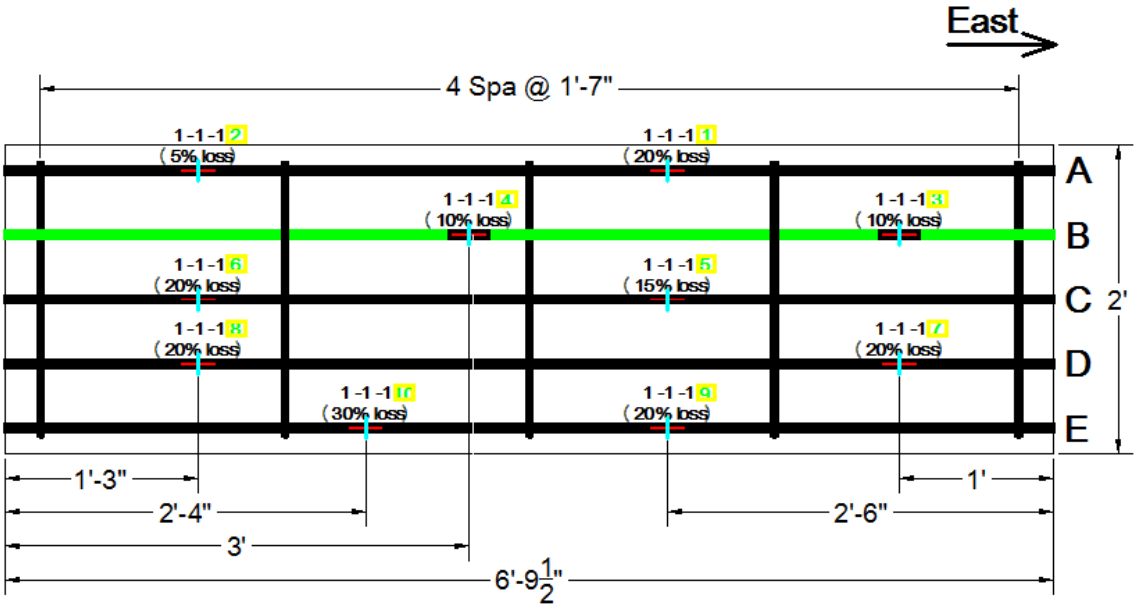

Figure 4.20: Top rebar layout for S2-1 with rebar B highlighted.

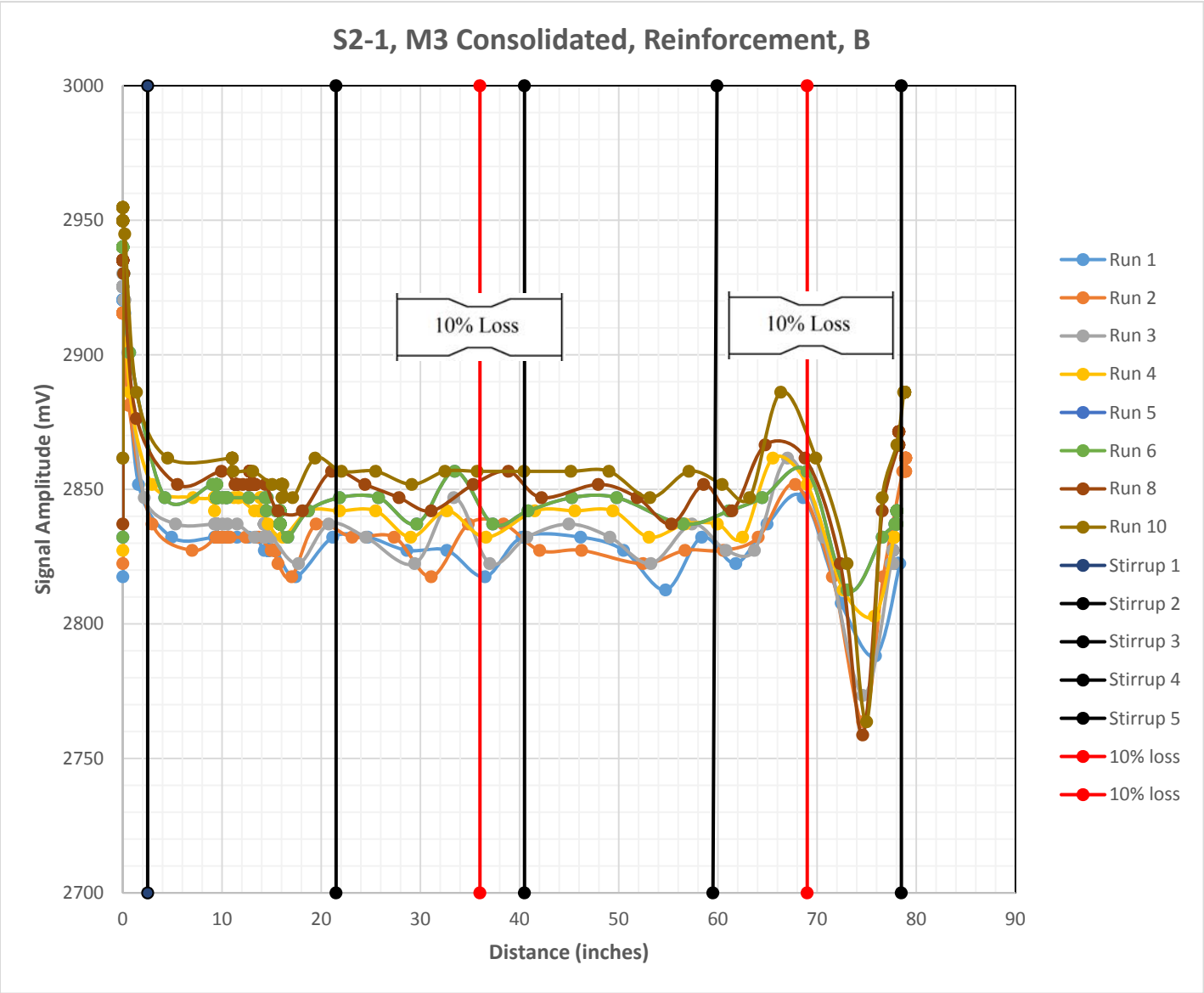

Figure 4.21: M3 Consolidated Graph for S2-1, Reinforcement Designated B, Top

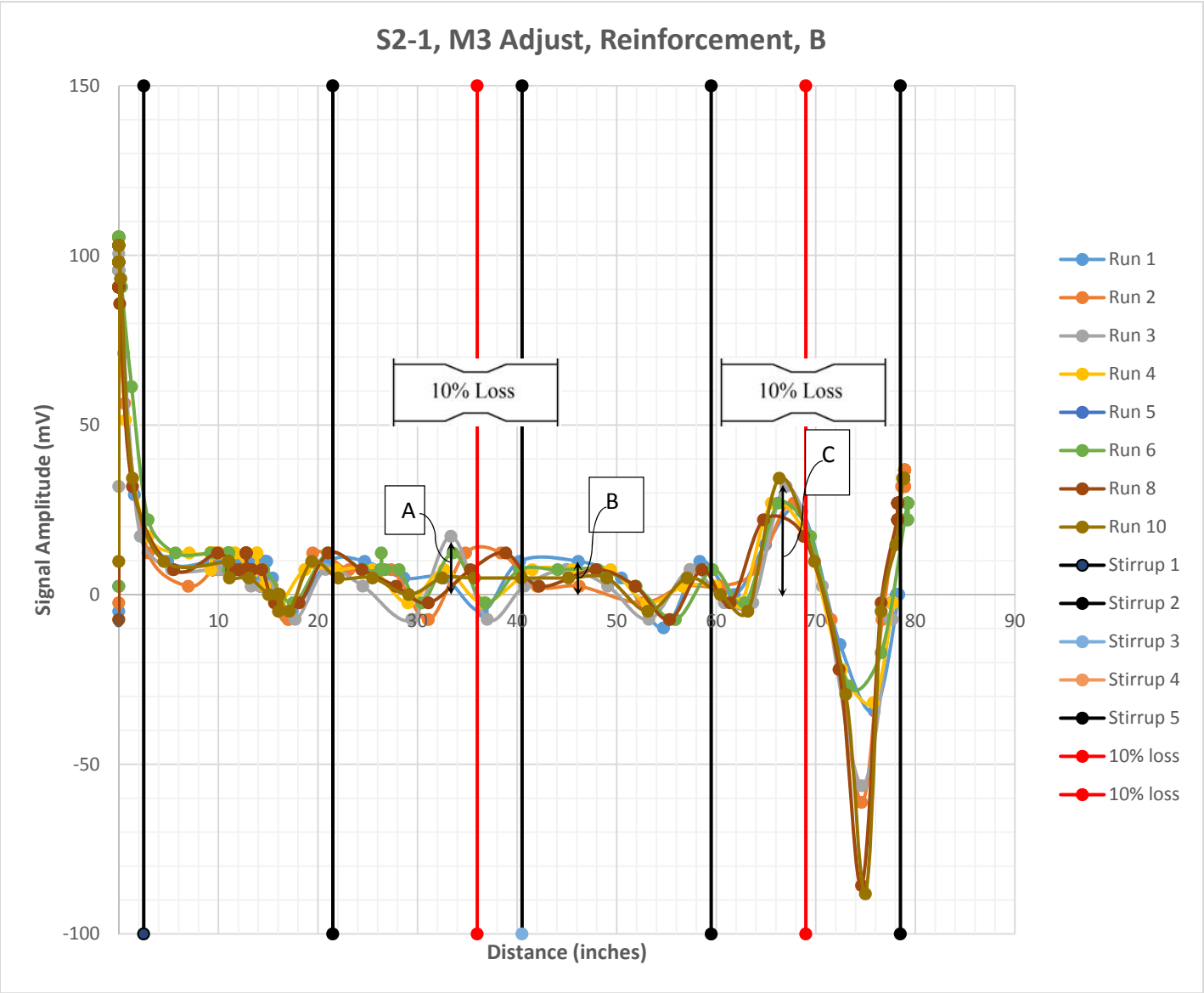

Figure 4.22: M3 Adjusted Graph for S2-1, Reinforcement Designated B, Top

Notation for Tables 4.4, 4.5 and 4.6

Location A = average +ve signal amplitude for 10% loss close to stirrup = 11.8 mV

Location B = average +ve signal amplitude between stirrups without loss = 7.8 mV

Location C = average +ve signal amplitude for 10% at center of stirrup = 28.7 mV

Change in signal amplitude at location A = 11.8 – 7.8 = 4.0 mV

Change in signal amplitude at location C = 28.7 – 7.8 = 20.9 mV

Using the generated quadratic equation: $y = 0.0263x^2 - 0.1976x + 2.9222$

where:

x = cross-sectional area loss in sq. inch

y = change in signal amplitude in milli-volts due to cross-sectional area loss and stirrup effect, eliminating the constant, the quadratic equation becomes $y = 0.0263x^2 - 0.1976x$.

Substituting the value of y at location A gives an approximate cross-sectional area loss of 0.02 in^2 considering a cross-sectional area of 0.3068 in^2 for #5 reinforcement, the approximate percentage loss in cross section is 6.5%. Substituting the value of y at location B gives an approximate cross-sectional area of 0.107 in^2 with an approximate percentage loss of 34.88%. The aproximate cross-sectional area loss at location A is considerably small compared to that at B. This was due to the proximity of the stirrup to the cross-sectional area loss at A compared to B.

The following were the findings from magnetic flux leakage analysis of scanned results from S2-1 top single layer reinforcement, S2-2 bottom double layered reinforcement with cross-sectional losses in the second layer and S2-3 top single layer strands. The results have been tabulated below.

Table 4.4 gives a summary results of similar calculations done for reinforcement B for the remaining designated reinforcement A, C, D and E showing the simulated percentage cross-sectional area loss in column 3 relative the predicted positive and negative change in millivolts using equation 4.1 from similar graphical representations as shown in Figures 4.21 and 4.22. Figures 4.24 and 4.25 show M3 Consolidated and M3 adjusted graphs for reinforcement H

at the bottom of S2-2 with grinding simulation 5-2-5 with cross-sectional area losses of 15% and 20%. Estimation losses have been detailed in Table 4.5.

Table 4.4: S2-1, Top Plan, Estimated Cross-sectional Area Loss

Stirrup spacing of 19", Single layer reinforcement, Cross-sectional loss configuration (1inch-1inch-1inch)

Rebar Designation	Defect location (West to East) (inches)	Simulated Cross-sectional Area Loss (%)	Change in (+) Amplitude (millivolts)	Estimated Cross-sectional Area Loss (in^2)	Estimated Cross-sectional Area Loss (%)
A	15	5	4	0.020	6.5
A	51.5	20	10	0.051	16.6
B	36	10	4	0.020	6.5
B	69.5	10	21	0.107	34.9
C	15	20	14	0.071	23.1
C	51.5	15	11	0.056	18.3
D	15	20	14	0.071	23.1
D	69.5	20	21	0.108	34.9
E	28	30	15	0.075	24.4
E	51.5	20	11	0.056	18.3

*Cross-sectional area of #5 reinforcement = 0.3068 in^2

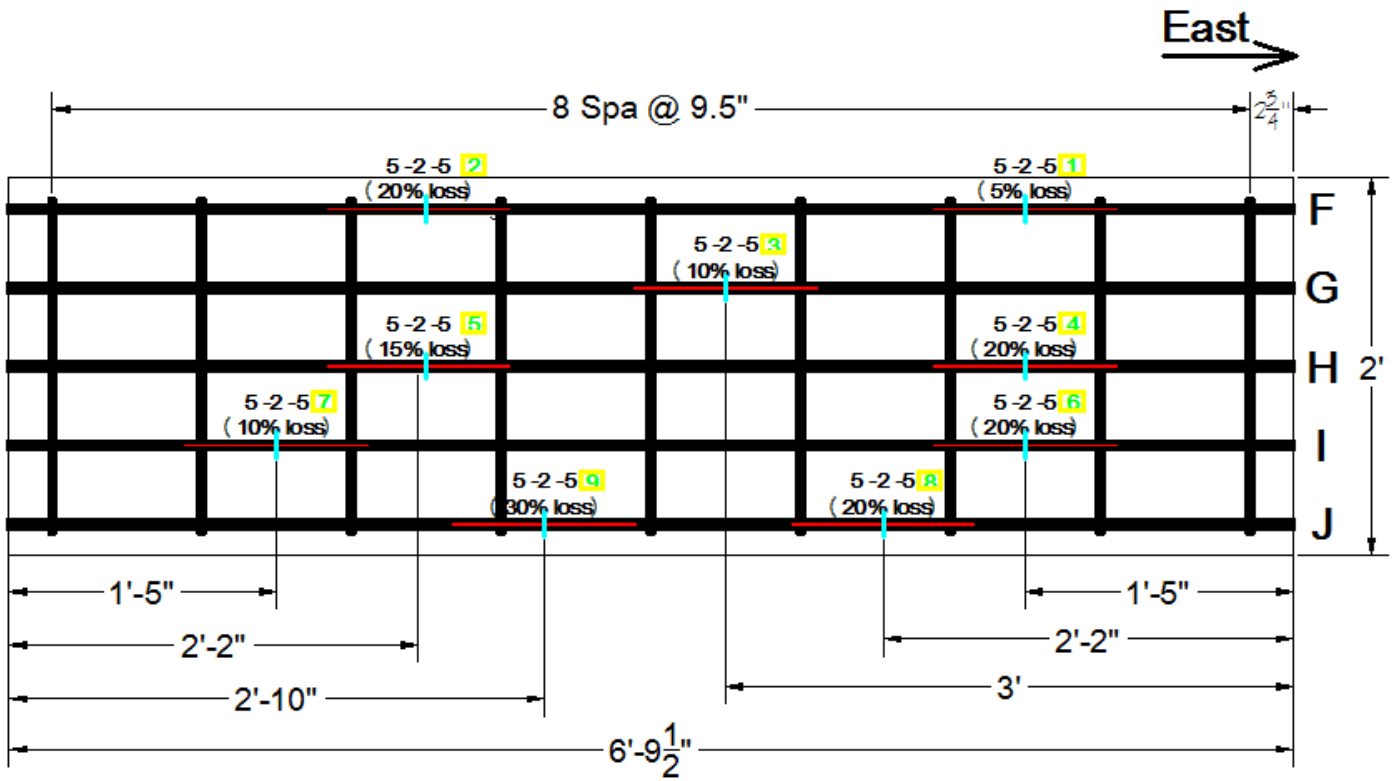

Figure 4.23: Bottom reinforcement layout for S2-2 with percentage cross-sectional losses

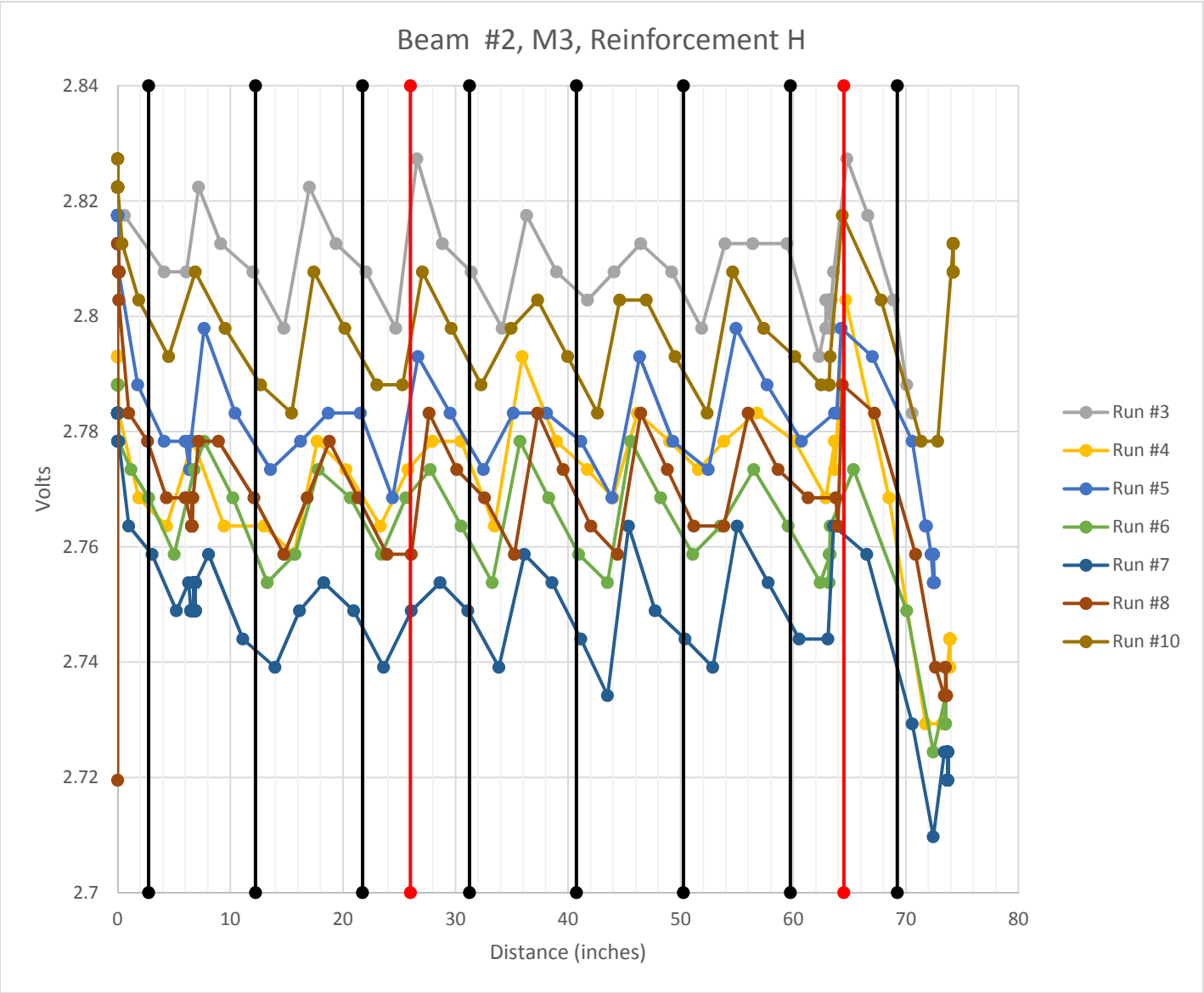

Figure 4.24: M3 Consolidated Graph for S2-2, Reinforcement Designated H, Bottom

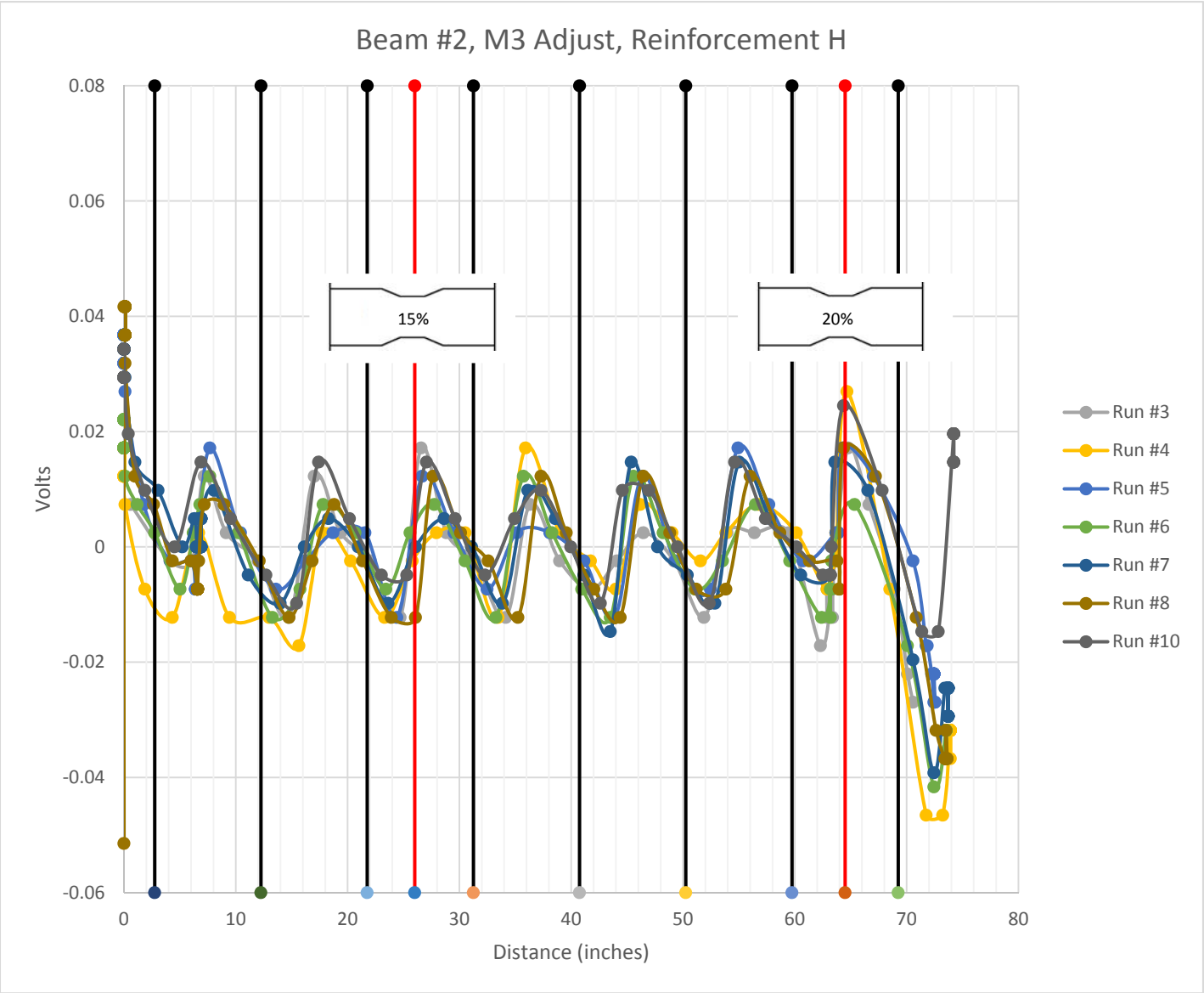

Figure 4.25: M3 Adjusted Graph for S2-2, Reinforcement Designated H, Bottom

Table 4.5: S2-2, Bottom Plan, Estimated Cross-sectional Area Loss

Stirrup spacing of 9.5", Double layer reinforcement, Cross-sectional loss configuration (5inch-2inch-5inch)

Rebar Designation	Defect location (West to East) (inches)	Simulated Cross-sectional Area loss (%)	Change in (+) Amplitude (millivolts)	Estimated Cross-sectional Area loss (in^2)	Estimated Cross-sectional Area loss (%)
F	26	20	5	0.025	8.1
F	64.5	5	9	0.045	14.7
G	45.5	10	9	0.045	14.7
H	26	15	6	0.030	9.8
H	64.5	20	12	0.060	19.6
I	17	10	6	0.030	9.8
I	64.5	20	9	0.045	14.7
J	34	30	3	0.015	4.9
J	55.5	20	10	0.050	16.3

*Cross-sectional area of #5 reinforcement = 0.3068 in^2

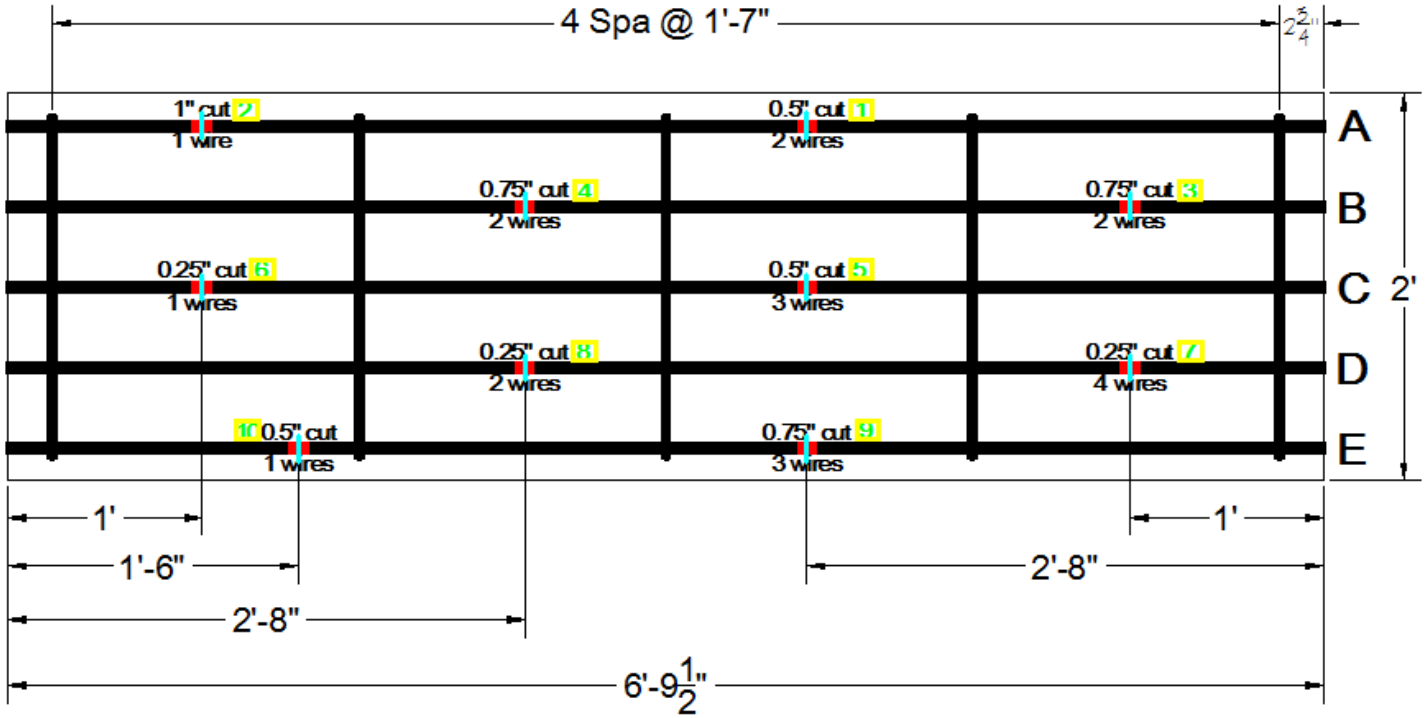

Figure 4.26: Top strand layout for S2-3 with number and length of wire cuts

Table 4.6: S2-3, Top Plan, Estimated Cross-sectional Area Loss

Stirrup spacing of 19", Single layer strands, Wire cuts

Strand Designation	Defect Location (West to East) (inches)	Length of Wire cut (inches)	Number of Wire cuts	Change in (+) Amplitude (millivolts)	Estimated Cross-sectional Area loss (in^2)	Estimated Cross-sectional Area loss (%)
A	12	1	1	5	0.025	16.3
A	49.5	0.5	2	12	0.060	39.2
B	32	0.75	2	5	0.025	16.3
B	69.5	0.75	2	5	0.025	16.3
C	49.5	0.5	3	6	0.030	19.6
D	32	0.25	2	10	0.050	32.6
D	69.5	0.25	4	5	0.025	16.3
E	18	0.5	1	10	0.050	32.6
E	49.5	0.75	3	5	0.025	16.3

*Cross-sectional area of 0.5" diameter strand = 0.153 in^2